12-2020

Optimizing Energy Power Consumption of Freight Railroad Bearings Using Experimental Data

Carlos Eliasar Lopez III
The University of Texas Rio Grande Valley

OPTIMIZING ENERGY POWER CONSUMPTION OF FREIGHT RAILROAD BEARINGS USING EXPERIMENTAL DATA

A Thesis

by

CARLOS ELIASAR LOPEZ III

Submitted to the Graduate College of
The University of Texas Rio Grande Valley
In partial fulfillment of the requirements for the degree of

MASTER OF SCIENCE IN ENGINEERING

December 2020

Major Subject: Mechanical Engineering

THEORETICAL AND EXPERIMENTAL STUDY ON THE ENERGY CONSUMPTION OF RAILROAD BEARINGS IN NORMAL AND ABNORMAL OPERATION CONDITIONS

A Thesis
by
CARLOS ELIASAR LOPEZ III

COMMITTEE MEMBERS

Dr. Constantine Tarawneh
Chair of Committee

Dr. Arturo Fuentes
Co-Chair of Committee

Dr. Horacio Vasquez
Committee Member

December 2020

ABSTRACT

Lopez, Carlos E., Optimizing Energy Power Consumption of Freight Railroad Bearings Using Experimental Data. Master of Science (MS), December 2020, 56 pp., 17 tables, 25 figures, 14 references.

Throughout the railway industry, trains use systems that record total energy efficiency of a train but not energy efficiency or consumption by components. Monitoring freight bearing power consumption can support the railroad industry efforts to maintain the railroad economic competitiveness and minimize the environmental impact.

For more than a decade now, the University Transportation Center for Railway Safety (UTCRS) at the University of Texas Rio Grande Valley (UTRGV) has been collecting power consumption data for railroad bearings under various loads, speeds, ambient temperatures, bearing condition, and bearing classes. Specifically, data such as temperatures, voltages, speed, and load were collected to perform an experimental analysis of the power consumption of a four-bearing axle. After obtaining an energy consumption profiles relative to the speed and load, each bearing was analyzed using the temperatures collected and theoretical values of conduction and convection to obtain an experimental value of power consumption. This paper will discuss the experimental setup and the comparison between estimations and findings of energy consumption of bearings as function of railcar load, train speed, condition of bearing, and bearing class whether it is healthy or defective, and type of defect.

DEDICATION

This thesis is dedicated to my family. Without your love, support, and guidance I would have never reached my dream of becoming an engineer. Without your sacrifices I would have never became the man I am today. All my accomplishments are thanks to you all.

ACKNOWLEDGEMENTS

My biggest thanks goes to Dr. Constantine Tarawneh. I am grateful for the opportunity to work for the center. Throughout the two years of working here I have learned an exponential amount in the field of engineering. Thank you for the support and guidance to becoming a better engineer and person. Without your hard work and dedication this center would never be as great as it is. Thank you for all the laughs, memories, and making me the person and engineer I am today.

Dr. Arturo Fuentes, thank you for your guidance throughout this research. Without your encouragement, enthusiasm, and insight this thesis would have not been possible.

Dr. Horacio Vasquez, thank you for always pushing me to do more. Your prospective helped mold the direction of this research.

To all my friends on the team, thank you for all the experiences, growth, and guidance. Vero, Joseph, Javi, and Jonas, thank you for all the help towards this research, and being available to answer any of my question.

Finally, this study was made possible by funding provided by The University Transportation Center for Railway Safety (UTCRS) , through a USDOT Grant No. DTRT 13-G-UTC59

DISCLAIMER

The contents of this thesis reflect the views of the authors, who are responsible for the facts and the accuracy of the information presented herein. This document is disseminated under the sponsorship of the U.S. Department of Transportation's University Transportation Centers Program, in the interest of information exchange. The U.S. Government assumes no liability for the contents or use thereof.

TABLE OF CONTENTS

Page

LIST OF TABLES

Page

LIST OF FIGURES

Page

CHAPTER I

BACKGROUND AND INTRODUCTION

1.1 Modern Freight Railroad Advancements

The railroad industry has played a vital role in the development of the United States. Over the years there has been great technological investments to the railroad, which made the railroads one of the most efficient forms of transporting goods for many miles with limited fuel consumption. In fact, literature shows that freight railroad competitiveness advantage is due to the following key factors which include reduction in friction that is created from the steel wheel assembly contacting the steel rail, engine efficiency advancements, and enhanced aerodynamics, among other factors [1]. These are among the main factors that kept the freight train industry more efficient than other competitors such as trailer trucks.

For example, a 500-mile freight train trip hauling 3000 tons would only consume 3185 gallons of diesel. Thus, making freight train performance at 471 ton-miles per gallon, which is about 3.5 times more efficient than the performance of trailer trucks [2].

Freight trains over the years have grown in technological advancements towards making the freight train industry safer and more efficient. This has been accomplished by using vast amounts of data while using smart sensors that are deployed across the network to create this massive database of information about the track and equipment conditions in the field. This data is used to identify combination of factors that can indicate if a piece of equipment is at its

lifespan and needs replacing before catastrophic failure. The technological enhancements seen in Figure 1 describe some of the on-hand controls and their location along the locomotive [3].

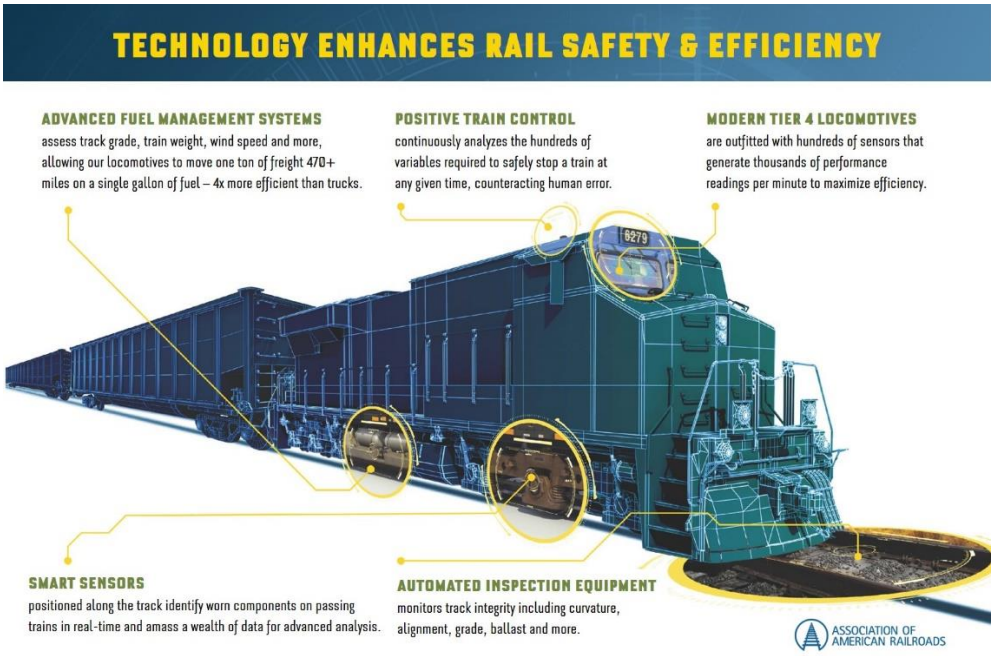

Figure 1: Technology enhances rail safety and efficiency [3]

Note that the smart sensors are utilized to identify worn components on passing trains in real-time. Even though this is a great feature to have in locomotives, the next logical step is to identify worn components on the rest of the train in real-time and monitor the efficiency of key components.

1.2 Trailer Truck Advancements

Over the past decade, there have been major efforts to improve the efficiency of trailer trucks. In some studies, researchers have suggested switching to electrical power trailer trucks, as well as to create self-driving trailers that have the ability to platoon with other trucks allowing them to travel with shorter distances between the trucks to improve the aerodynamics, thus, making them more fuel efficient [4-5]. An example of platooning is illustrated in Figure 2. The technology that allows platooning is relatively new. Studies have been conducted to find the

percentage of trucks on the highway that are both capable of and would benefit from platooning, and that was found to be 71-80% [6]. Studies have also concluded that platoons consisting of three closely following trucks can save a combined 13% on fuel consumption, which would result in savings close to 2.1 billion gallons of fuel per year [6]. Hence, platooning can have a positive impact on fuel economy and environmental pollution.

In 2015, nearly 18.1 billion tons of goods worth around $19.2 trillion were transported throughout the United States. Of the 18.1 billion tons, 63% of the tonnage was transported by truck and 10% was transported by rail. For the next 30 years, there is expected growth in the value of shipments, thus, there is value to make these forms of transportation as efficient as possible.

Trucks are more cost effective for short distance deliveries, however, with this advantage there are consequences. Throughout the years of 2014 through 2018 an average of 3,663 fatalities involving trailer trucks would happen each year. Throughout that same time frame, an average of only seven deaths per year was recorded for freight trains [7-8].

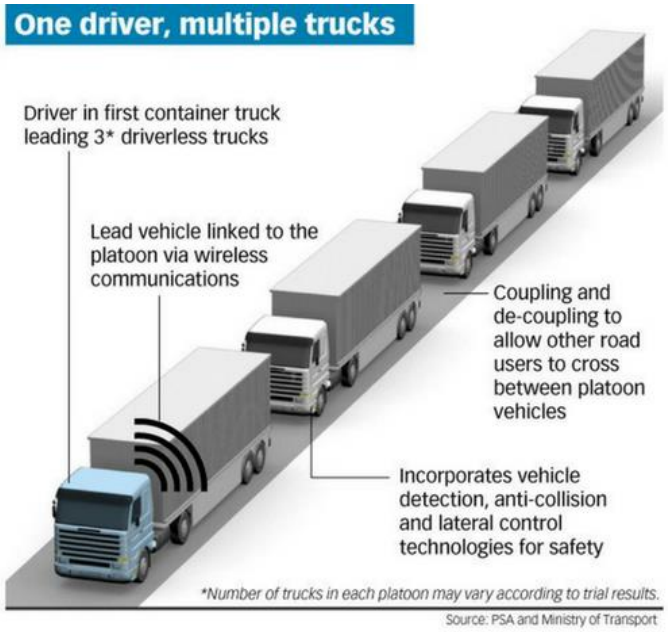

Figure 2. Platooning technology [9]

1.3 Bearing Defects

For freight trains to remain a viable competitor to trailer trucks, constant enhancements and advancements must be made to maintain the competitive edge. A mixture of analytical models coupled with experimental testing can yield favorable results to ensure that trains are performing optimally. Some current analytical modeling of railroad fuel consumption involves a multi-step process. One of the initial steps in the process is being able to estimate the required number of locomotives needed to effectively move the train to its destination. Calculating the fuel consumed during acceleration and determining the resistance forces are other steps in this process. There are several equations that have been developed and are widely used in the field. These equations consider the resistance from drag force which varies with speed, along with wheel rolling resistance, flange resistance, among other factors. Note that these equations assume the tapered roller bearing resistance to be constant and not varying with speed [10], which is not

the case. The lack of experimental testing and analysis performed solely on the bearing is the reason behind the simplified models used. Hence, rigorous experimental testing is essential for quantifying the frictional heating within a bearing as a function of speed to optimize the fuel efficiency.

To date, very few power consumption studies targeting specific railroad components have been performed. To address this, the University Transportation Center for Railway Safety (UTCRS) research team has been investigating the power consumption of railroad tapered-roller bearings. The ongoing work presented in this thesis focuses on finding correlations for the bearing power consumption as a function of load, speed, ambient temperature, and bearing condition.

1.4 Tapered Roller Bearings

The conditions of the individual freight railcar can also significantly impact the fuel efficiency of the total system. Fright railcar suspension consists of several components: side frames, springs, dampers, wheels, axles, and tapered roller bearings. Of these components, the bearings are the most susceptible to develop defects at high speeds under heavy cargo loads [11]. The fundamental components of a railroad bearing are the rollers, inner rings (cones), and outer ring (cup), shown in Figure 3.Under optimal operating conditions, these components have relatively low power consumption. However, their effectiveness can be compromised under abnormal operating conditions resulting from defects that exist or develop within the bearing. These defects can be categorized into three different categories: localized defects, geometric defects, or distributed defects. Two examples of localized defects are illustrated in Figure 4 (left). Localized defects can range from pits, cracks, or spalls on a single component of the bearing. These localized defects can cause multiple bearing components to form defects

transitioning to a distributed defect. Distributed defects can also be found on a single component with multiple defects throughout its rolling surface such as a water-etch defect, illustrated in Figure 4 (right). Water-etch usually results from a compromised seal on the bearing allowing water or moisture to get inside the bearing and degrade the lubricating grease. Once enough grease is degraded, it leads to increased metal-to-metal friction, amplifying the wear and tear and further decreasing the effectiveness of the bearing lubricant. Finally, geometric defects are those resulting from manufacturing tolerance errors or caused by abnormal wear of the rolling surfaces.

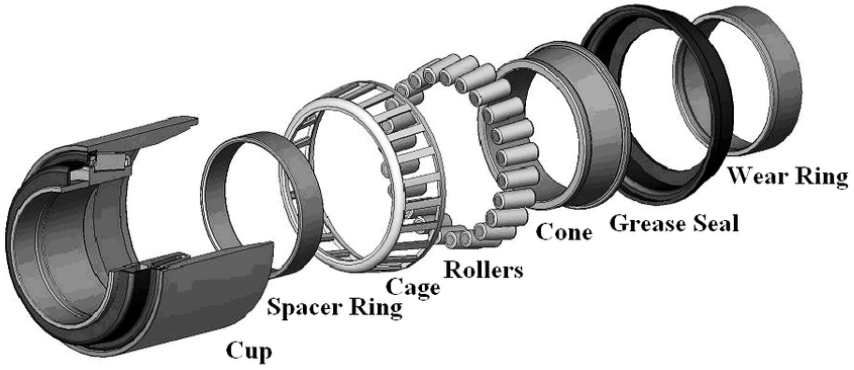

Figure 3. Components of a tapered roller bearing

Deformations in the rollers, cups, or cones can result in an increase in frictional heating especially if the bearing develops a defect on any of the raceways [12]. There are two bearings per axle and four axles per wagon in a typical freight railcar. Freight trains can haul up to 59 wagons, which corresponds to a total of 472 bearings. When hauling up to 18,000 tons, even a small change in the condition of the bearings can potentially result in significant differences in the energy efficiency.

Figure 4. Example of localized defects (left) and distributed defect (right)

CHAPTER II

EXPERIMENTAL SET UP AND INSTRUMENTATION

To replicate bearing operation in freight railcars, the University Transportation Center for Railway Safety (UTCRS) designed and fabricated three dynamic bearing testers, housed at UTRGV. Two of these testers were utilized to perform all laboratory experiments for this study. These testers can accommodate Association of American Railroads (AAR) class E (6" × 11"), class F (6 ½" × 12"), class G (7" × 12"), and class K (6 ½" × 9") tapered-roller bearings. The experiments conducted for this study utilized class F and K bearings only. The bearings for this study were tested on two of three dynamic test rigs housed at UTRGV, which are: the four-bearing tester (4BT) and the chamber four-bearing tester (C4BT) pictured in Figure 5 and Figure 6 respectively. Each tester is equipped with a hydraulic cylinder that can apply up to 150% of the full AAR load rating for a class F or K bearing, which is 153 kN (34.4 kip) per bearing. The data used in this study was acquired from laboratory experiments that were carried out at 17% load (26 kN or 5.85 kips) per bearing corresponding to an empty railcar and 100% load (153 kN or 34.4 kips) corresponding to a fully loaded railcar. The dynamic testers utilize a 22 kW (30 hp) variable speed motor powered by a variable frequency drive (VFD) that is used to simulate the different train speeds up to 137 km/h (85 mph), listed in Table 1. To simulate the convection cooling effect of the crosswind on the railroad bearings in a moving train, two to three industrial size fans that produce an average airflow of 6 m/s (13.4 mph) over the test bearings were utilized, as pictured in Figure 5 and Figure 6.

Figure 5. Four-Bearing Test Rig (4BT)

Figure 6. Chamber Four-Bearing Test Rig (C4BT)

Table 1. Typical speeds used to perform the experiments for this study.

Axle Speed [rpm]	Track Speed [mph]	Track Speed [km/h]
280	30	48
420	45	72
498	53	85
560	60	97
618	66	106
799	85	137

2.1 Bearing Assembly

Class F and K bearings were chosen for this study because these two classes of bearings represent about 90% of all freight railcar bearings used in North America. Both classes are fabricated using AISI 8620 steel and have the tapered rollers case-hardened. The difference between these two classes of bearings is the total width of the outer ring (cup). Class K bearings have a shorter cup width than class F bearings by about 2.34 cm (0.92 in). Consequently, a shorter spacer ring is needed for class K bearings. Class K spacer rings are approximately 1.46 to 1.48 cm (0.575 to 0.583 in) while class F spacer rings are between 3.68 and 3.94 cm (1.45 to 1.55 in). Additionally, less grease is used when building class K bearings since no grease is applied in the spacer ring region as opposed to class F bearings. Hence, class K bearings are a little lighter than their class F counterpart.

2.2 Lubrication

Each bearing tested is assembled and lubricated following the Association of American Railroad (AAR) standards. The grease quantities and application locations within the bearing are specified in Table 2. Since both class F and K bearings use identical cone assemblies, the grease applied to each cone assembly is the same. In Table 2, the amount of grease listed under the cone assembly is divided equally among the two cone assemblies within each bearing (i.e., each cone assembly receives 192.25 mL or 6.5 oz). As mentioned earlier, class F bearings have a longer spacer ring region than class K bearings. Therefore, 266.2 mL (9 oz) of grease is applied to the spacer ring region of class F bearings while none is applied to the corresponding region in class K bearings.

Table 2. Lubrication (grease) application for class F and K bearings

Bearing Class	Total Grease Applied [mL] / [oz]	Spacer Region Grease [mL] / [oz]	Cone Assembly Grease [mL] / [oz]
F	650.6 / 22	266.2 / 9	384.5 / 13
K	384.5 / 13	N/A	384.5 / 13

After the appropriate amounts of grease are applied as specified in Table 2, the bearing is secured with seals on each end of the bearing to prevent grease from leaking out of the assembly and safeguard against water or dirt from entering the bearing. The bearing is then weighed to ensure that it has been properly lubricated and to have a reference weight to compare against when the experiment is completed. Class K bearings weigh on average about 30 kg (66 lb) while class F bearings weigh on average about 35.4 kg (78 lb). Note that the weight of bearings varies based on the type of cage used in the cone assembly. The values given above correspond to cone

assemblies that utilize polyamide (polymer based) cages which are significantly lighter than their counterpart steel cages. For consistency, all the laboratory experiments performed for this study utilized cone assemblies built with polyamide cages.

2.3 Laboratory Test Rigs

2.3.1 Four-Bearing Tester (4BT) & Chamber Four-Bearing Tester (C4BT)

The four-bearing tester (4BT) and the chamber four-bearing tester (C4BT) can accommodate four class E, F, G, or K railroad bearings pressed onto a customized test axle. Both testers are nearly identical in their design and fabrication. However, there are two main differences between the two test rigs.

First difference is that one of these four-bearing testers is housed with a specially designed environmental chamber that is equipped with a 2-ton fan-coil chiller unit that is capable of providing ambient temperatures in the range of -40°F to 140°F. This feature allows researchers to simulate different ambient temperatures ranging from normal to extreme conditions that freight trains may experience in field service. To expedite laboratory testing conducted in the C4BT, the bearings are run utilizing two main operating conditions, namely, 85 km/h (53 mph) at 17% load and 137 km/h (85 mph) at 100% load.

The second difference between the 4BT and the C4BT relates to the pulley systems used in each tester. The two pulley systems utilized are illustrated in Figure 7 with each component described in Table 3. The main difference is that the C4BT utilizes a pulley system with a belt tensioner which can vary the tension in the belts by laterally torqueing a customized smaller pulley system. In the 4BT, the tension is varied by adjusting the height placement of the drive motor through the addition or removal of steel shims of different thickness, thus, eliminating the need for the belt tensioner used in the C4BT.

To simulate field service conditions, only data collected from the middle two bearings was used in this study because these bearings are top loaded (refer to Figure 8) as is the case in field service. The tester configuration in both the 4BT and the C4BT is identical with the load being equally applied to the middle two bearings on the test axle through the load cell and an I-beam that spans the length of the two middle bearings. The two outer bearings on the test axle counteract the applied force providing an equal distribution of applied load on all four bearings. Hence, at full load (100%), the load applied per bearing is 153 kN (34.4 kips), whereas, at 17% load (empty railcar load), the load applied per bearing is 26 kN (5.85 kips), with the two middle bearings being top loaded and the outer two bearings being bottom loaded.

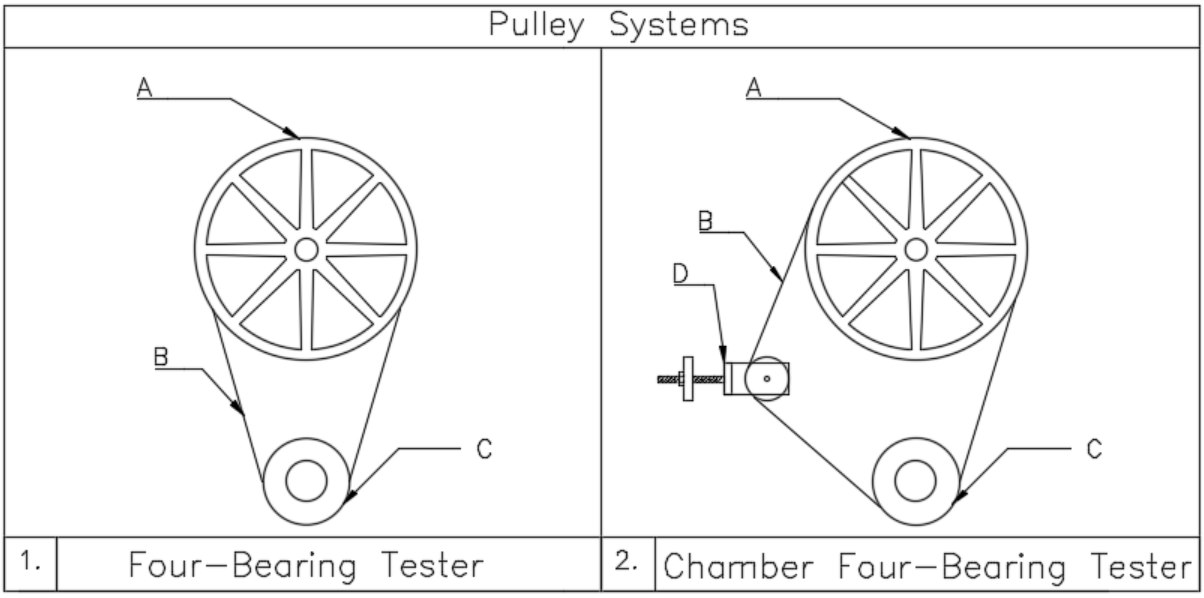

Figure 7. Schematic diagram showing the different pulley systems used.

Table 3. List of components for pulley systems illustrated in

Pully Components	
A	Driven Pulley (connected to test axle)
B	Three Belts
C	Diver Pulley (connected to motor)
D	Secondary Pulley (provides tension)

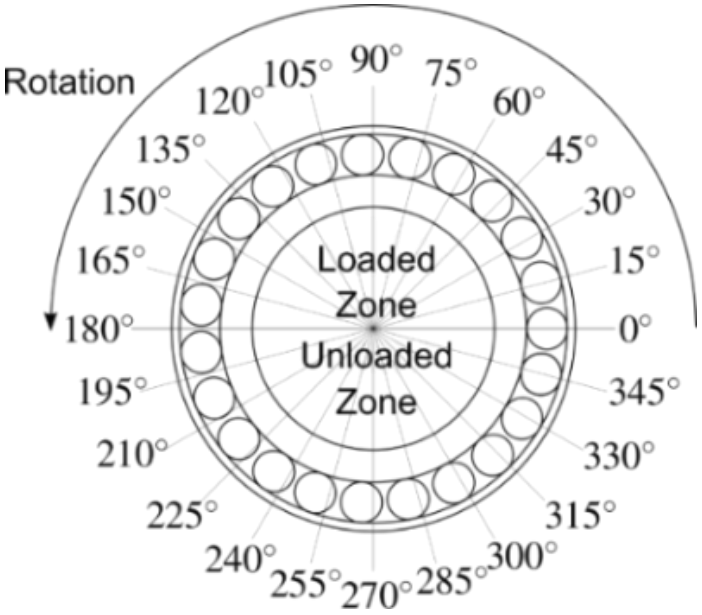

Figure 8. Schematic diagram showing the loading zones

2.3.2 Instrumentation

Figure 9 shows the locations of the three accelerometers used to acquire the vibration signatures within the bearing. These locations are the Smart Adapter (SA), Mote (M), and Radial (R) location. The steel adapters for the middle two bearings (B2 and B3) were each machined to accommodate two 70g accelerometers affixed to the SA and M locations, a 500g accelerometer placed on the R location, and two bayonet-style K-type thermocouples affixed to the bearing adapter and aligned with the middle of each cup raceway. Additionally, a regular K-type

thermocouple was also instrumented. This thermocouple was aligned with the two bayonet thermocouples and placed in the middle of the bearing cup width and held in place by a hose clamp. A schematic diagram of the test axle along with sensor locations is provided in Figure 10.

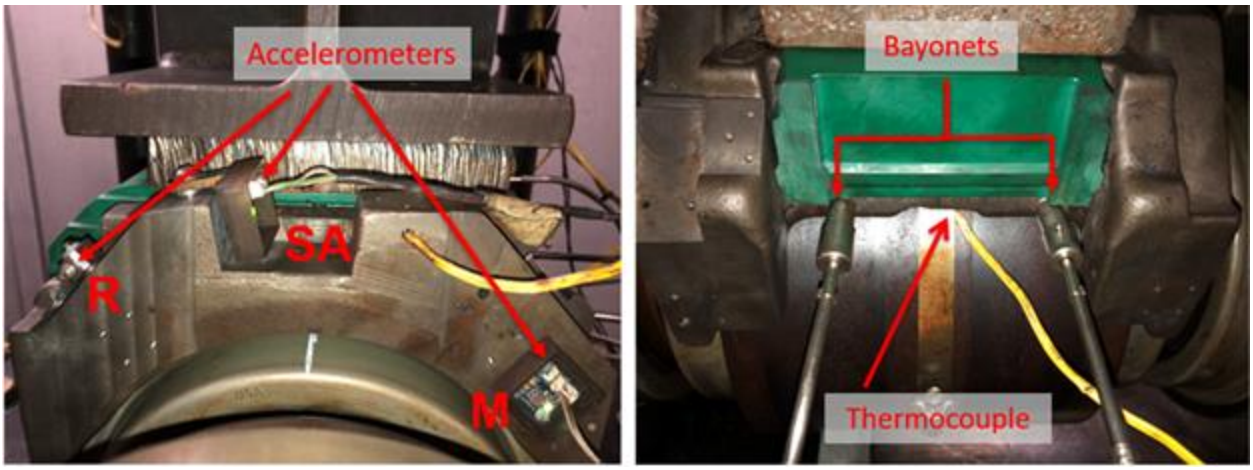

Figure 9. Modified bearing adapter showing sensor locations

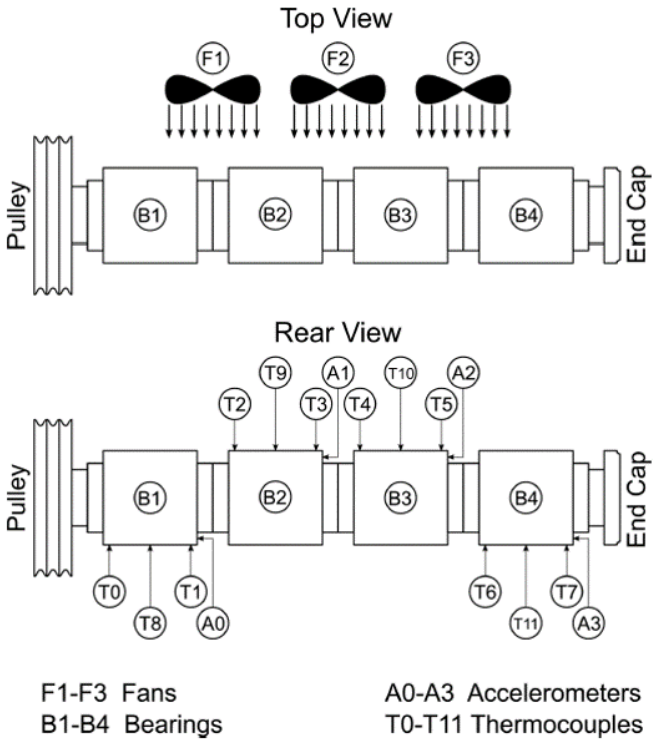

Figure 10. Top and rear views of 4BT configuration including sensor locations

A National Instruments (NI) PXIe-1062Q data acquisition system (DAQ) programmed using LabVIEW™ was utilized to collect the data for this study. A NI TB-2627 card was used to record the thermocouple temperature readings at a sampling rate of 128 Hz for 0.5 seconds in twenty-second intervals. A combination of a NI 9239, a NI USB-6008, and a NI 9234 cards were used to record and collect the accelerometer data for this study at a sampling rate of 5,120 Hz for sixteen seconds, in ten-minute intervals. Lastly, a NI 9205 card was used to record the motor power consumption readings at a sampling rate of 100 Hz for 0.5 seconds in twenty-second intervals.

CHAPTER III

METHODOLODIES

3.1 Bearing Assembly

The following power consumption calculations were performed neglecting the small energy losses through the tester's pulley system which enables power transfer from the motor to the test axle. In turn, this computation process is essential as it permits the conversion of experimental power consumption into gallons of diesel [13]. First, the fuel flow rate to the engine is calculated using Eq. (1) as follows,

$$\dot{m} = \frac{b_e \cdot P_e}{3600 \frac{s}{h} \cdot 1000 \frac{g}{kg}} \tag{1}$$

where $\dot{m}$ is fuel flow rate to the engine in [kg/s], b_e is brake specific fuel consumption of the engine in $[g/kWh]$ (assumed 224 g/kWh) [12], and P_e is the engine power in $[kW]$. Then, Eq. (2) is used to estimate the gallons of diesel as follows,

$$G = \dot{m} * t_e * 0.3105 \frac{gallon_{diesel}}{kg} \tag{2}$$

where *G* is the gallons of diesel, and t_e is the total running time of the experiment in seconds. Now, to calculate the miles per gallon (MPG) and the ton-mile per gallon values presented in this study, the following equations are used,

$$MPG = \frac{Total\ Miles\ Run}{G} \tag{3}$$

$$\frac{ton \cdot mile}{gallon} = \frac{MPG \times Load\ in\ lb_f}{2000\ lb_f\ per\ ton} \quad (4)$$

It is also important to mention that the experimental results presented in this study do not account for the resistance caused by drag forces. Additionally, the results presented include simulations of the power consumption and energy efficiency of all the bearings within the train based on the number of wagons proposed. Each simulated wagon contains four axles for a total of eight bearings per wagon. Therefore, to simulate one wagon, the experimental power consumption obtained from this study is doubled since the experimental setup allows for only four bearings on the test axle. In addition, when one of the four bearings on the test axle is defective, the simulation considers that 25% of the wagon's bearings are defective.

3.2 Chamber Four-Bearing Tester and Four-Bearing Tester

A relevant correlation between power consumption and bearing operating temperatures can be devised by tracking the temperature histories of test bearings running on both the four-bearing tester (4BT) and the chamber four-bearing tester (C4BT). Hence, this correlation can be utilized to estimate the power consumption of the four bearings on each test axle.

For this estimation to be as accurate as possible, several measures must be taken to avoid discrepancies in the collected data. For instance, control (i.e., defect-free or healthy) bearings must be allowed to reach steady state operating conditions for the experimental data to be used in the estimated power consumption calculations. Moreover, only the temperature difference above ambient for all four test bearings must be considered in the correlation since no power consumption is needed to maintain the bearings at the ambient temperature. Finally, since the motor power consumption recorded is the result of running all four test bearings, it needs to be

correlated to the cumulative temperature difference above ambient (ΔT_c) of all four test bearings, as follows:

$$\Delta T_c = \Delta T_{B1} + \Delta T_{B2} + \Delta T_{B3} + \Delta T_{B4} \quad (5)$$

where ΔT_{B1}, ΔT_{B2}, ΔT_{B3}, ΔT_{B4} represent, respectively, the temperature differences above ambient for test bearings B1, B2, B3, and B4 (refer to the schematic of Figure 10).

An example of this methodology is presented in Figure 11. This figure illustrates the four-bearing tester (4BT) running four class K control bearings (i.e., healthy bearings with no defects) operating at 100% load (i.e., 153 kN or 34.4 kips per bearing) simulating a fully loaded railcar with a track speed of 137 km/h (85 mph). A close inspection of this figure reveals similar trends between the motor power consumption and the temperature differences above ambient from all four bearings.

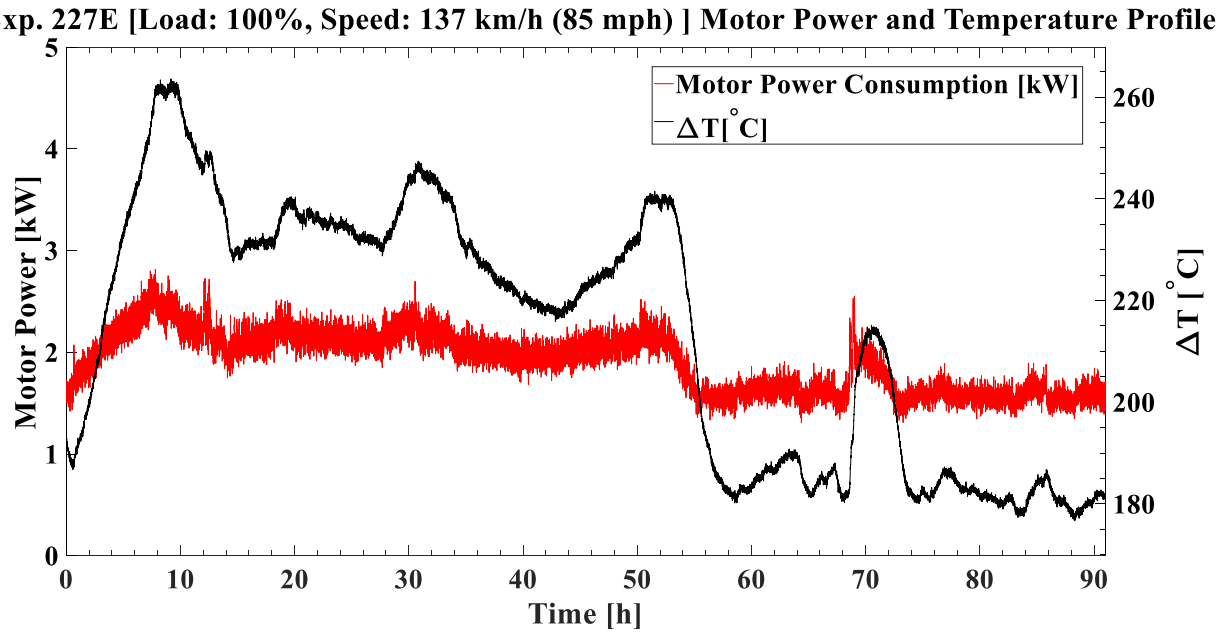

Figure 11. Motor power and temperature profile at 100% load and a track speed of 137 km/h (85 mph) on the 4BT running four class K bearings.

To obtain motor power estimates from the total temperature difference above ambient,

the total temperature difference must be scaled down to match the power consumption. To do so, the motor power consumption is divided by the temperature difference to generate a scale multiplier referred to as the scale factor. Note that different scale factors will be generated for both the four-bearing tester (4BT) and the chamber four-bearing tester (C4BT) as well as for the different speed and load conditions run on each tester. These scale factors are described in detail in Section 3.2.1 and Section 3.2.2.

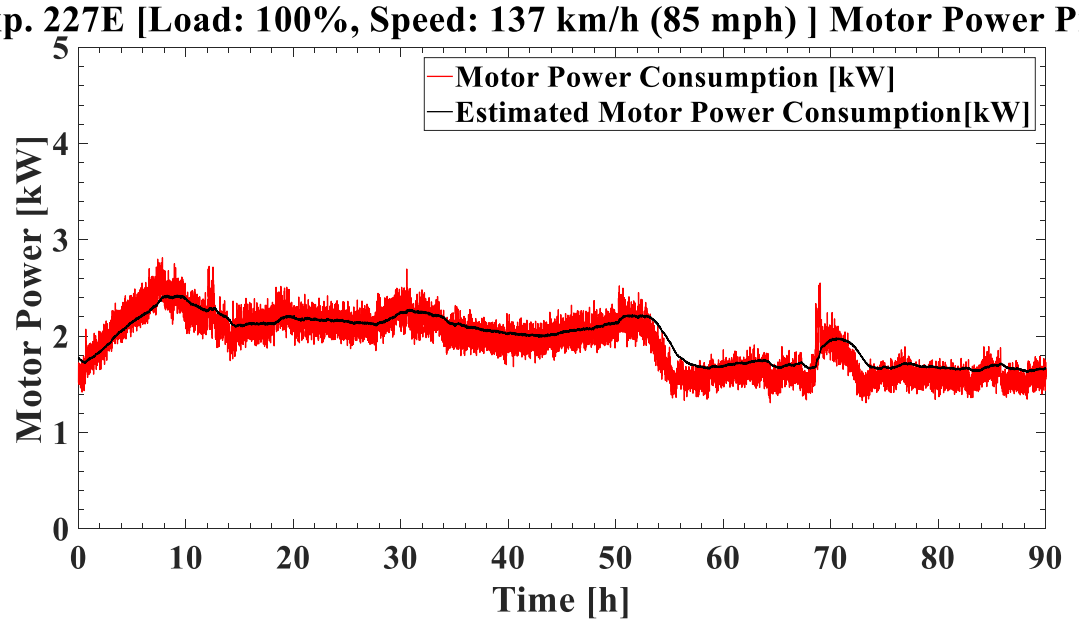

Figure 12. Motor power profile at 100% load and a track speed of 137 km/h (85 mph) on the 4BT running four class K bearings.

Multiplying the temperature profile by the acquired scale factor results in the behavior seen in Figure 12. The temperature profile is now scaled and closely resembles the motor power profile; however, a time lag between the motor power and the temperature profiles is also present. To determine this time delay (also referred to as time shift), the coefficient of determination (R^2) value of a few different time shifts is compared for several experiments, as listed in Table 4. Because the R^2 value is numerically determined and represents dataset

adaptation to a linear regression model, this analysis will also be used to quantify the agreement between the estimated motor power consumption model and the actual power consumption profile. Note, the closer the R^2 value is to 1, the better the two profiles match one another. In addition to using the R^2 value, a percent error calculation, given in Eq. (6), will also be used to assess the accuracy between the estimated power consumption model and the actual motor power consumption. Both analytical tools will provide a measure for the accuracy and reliability of the estimated power consumption results presented in this study.

$$\%\text{Error} = \frac{|P_A - P_E|}{P_S} * 100\% \tag{6}$$

Where P_A $[kW]$ is the actual power consumption, and P_E $[kW]$ is the estimated power consumption obtained through the developed model.

Table 4: R^2 values of several time shifts for different experiments

Quantifying Time Shift (i.e., Time Delay)									
Experiment	Load	Speed	R^2 Value						
220	100	280	0.14	0.13	0.13	0.13	0.13	0.14	0.15
220	100	420	0.49	0.50	0.50	0.50	0.50	0.51	0.50
220	100	498	0.52	0.43	0.54	0.54	0.53	0.54	0.54
220	100	560	0.14	0.15	0.16	0.17	0.19	0.20	0.21
220	100	618	0.36	0.38	0.39	0.40	0.41	0.42	0.42
220	100	798	0.40	0.43	0.46	0.46	0.46	0.43	0.42
230E	100	798	0.91	0.91	0.91	0.91	0.92	0.92	0.92
227E	100	798	0.84	0.85	0.85	0.85	0.85	0.86	0.86
227D	100	798	0.95	0.95	0.95	0.95	0.95	0.95	0.95
Time Shift (min)			0	15	30	45	60	75	90

Table 4 summarizes the R^2 values for different time shifts ranging from 0 to 90 minutes in 15-minute increments. Looking at this data, it can be seen that the R^2 values begin to stabilize after 30 minutes, which implies that it takes the bearings about 30 minutes to feel the thermal

effects of changes in power consumption. This finding agrees with previous studies performed on the thermal response of railroad tapered-roller bearings published elsewhere [14]. Note that larger time shifts have diminishing returns and are not practical in field service since freight trains cannot maintain constant speeds for long periods. Therefore, the selected time shift used for the data presented in this study will be 30 minutes.

Now that an appropriate time shift has been selected, it is prudent to also refine the actual power consumption profiles. This step can be accomplished using the smooth function in the mathematical software MATLAB®. This process decreases the number of small deviations in the actual motor power data providing a more efficient method to correlate the temperature profiles with the motor power consumption. Since the motor power data is collected every 20 seconds, the smooth function will be utilized to provide a moving average of 90 consecutive data points, which corresponds to the 30-minute time shift (or time delay) selected earlier.

Figure 13 illustrates the effects of using the smooth function in MATLAB® on the motor power consumption. A noticeable decrease in the motor power consumption deviations can be observed as a result of smoothing when compared to the raw (i.e., unsmoothed) data collected. Hence, smoothing the raw data by utilizing the 90-data-point moving average allows for a better, more accurate, and more efficient comparison between the actual motor power consumption and the estimated motor power consumption acquired from the developed model. For consistency, all actual motor power consumption profiles presented in this study will be those of the smoothed data.

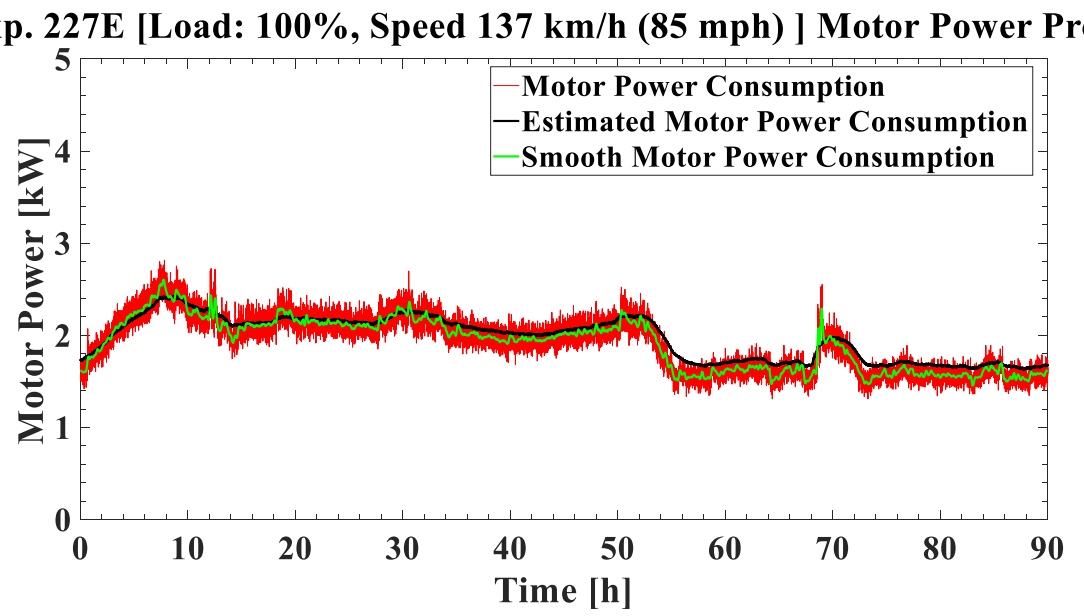

Figure 13: Motor power profile at 100% load (full railcar) and 137 km/h (85 mph) run on the 4BT using lass K bearings

3.2.1 Chamber Four-Bearing Tester (C4BT)

The chamber four-bearing test rig experiments were performed using both class F and K bearings. Class F bearings were tested at: 17% load (empty railcar) with a speed of 85 km/h (53 mph) and 100% load (fully loaded railcar) at speeds of 85 km/h (53 mph) and 137 km/h (85 mph). Class K bearings were tested at: 17% load (empty railcar) with a speed of 85 km/h (53 mph) and 100% load (fully loaded railcar) at a speed of 137 km/h (85 mph). For experiments run at 17% load, a single scale factor was used to correlate bearing operating temperature to power consumption since the bearings were run at one speed only.

Because temperature and power consumption usually require about two hours to reach steady state conditions after a sudden change in operating conditions, the first two hours of experimental data after any change in operating conditions was ignored. After the second hour, every 15 minutes of data was averaged until the fifth hour of the experiment was reached.

Between the second and fifth hour, a maximum and a minimum value for both the bearing operating temperature difference above ambient and the motor power were obtained. After these maximum and minimum values were collected, the motor power values were divided by the respective temperature difference values resulting in scale factor values. The scale factor values were then averaged to produce a single value. This process was repeated for every combination of speed and load tested for each bearing class.

The scale factor results for the class K experiments are as follows: at 17% load and a speed of 85 km/h (53 mph), the scale factor was 0.0213, whereas at 100% load and a speed of 137 km/h (85 mph), the scale factor was 0.0184. These scale factors were then multiplied by the respective cumulative bearing operating temperature difference above ambient (ΔT_c) for all four bearings on the test axle to compute the estimated motor power profiles.

As for the class F bearing experiments performed at 17% load and a speed of 85 km/h (53 mph), the scale factor was determined to be 0.0219, whereas at 100% load and speeds of 85 km/h (53 mph) and 137 km/h (85 mph), the scale factor was found to be 0.0174 and 0.0149, respectively.

3.2.2 Four-Bearing Test Rig (4BT)

In contrast to the chamber tester (C4BT) experiments which involved the implementation of both class F and K control (i.e., healthy) bearings [Section 3.2.1], the four-bearing tester (4BT) experiments were performed using only class K control (healthy) bearings. In addition, although the 4BT experiments were also conducted under loads of 17% (empty railcar) and 100% (fully loaded railcar) like the C4BT experiments, the 4BT experiments encompassed a range of simulated train speeds between 48 km/h (30 mph) and 137 km/h (85 mph). Note that the steady-state transition protocol followed for the C4BT experiments also applies for the 4BT tests.

Hence, the first two hours of data after any sudden changes in operating conditions was ignored, and only steady state data was used for the analysis. Employing this methodology and following the data analysis procedures delineated in Section 2.3.1, the collected steady state 4BT data was analyzed to determine the appropriate scale factors.

Figure 14 and Figure 15 display the scale factors for the disclosed speed range at both loading conditions of 17% (empty railcar load) and 100% (full railcar load), respectively. To illustrate a possible correlation between the selected train speed range and the corresponding scale factors, a first and second order polynomial equation regression models were applied. For the case of an empty railcar load (17% load), the behavior characterized by the linear regression model and its respective R^2 value suggests that a second order polynomial equation is a better fit. However, for the case of a fully loaded railcar (100% load), the difference between the linear and second order regression models was negligible, as evident by the R^2 values of both fits. Nevertheless, the second order regression models were used to determine the appropriate scale factors.

The scale factors (SF) can be determined by the second order polynomial given by Eq. (7) for an unloaded railcar (empty railcar) and by Eq. (8) for a loaded railcar (full railcar) as follows:

$$SF_{ul} = 1.2 \cdot 10^{-6} \cdot V^2 - 1.9 \cdot 10^{-4} \cdot V + 1.8 \cdot 10^{-2} \quad (7)$$

$$SF_{fl} = 3.6 \cdot 10^{-7} \cdot V^2 - 1.0 \cdot 10^{-4} \cdot V + 1.5 \cdot 10^{-2} \quad (8)$$

Where V is the simulated train speed in [mph], SF_{ul} is the scale factor for an unloaded railcar (empty railcar) in $[\frac{kW}{K}]$, and SF_{fl} is scale factor for a fully loaded railcar in $[\frac{kW}{K}]$. Equations (7) and (8) provide a simple method to estimate the appropriate scale factors when a

freight train is changing speeds.

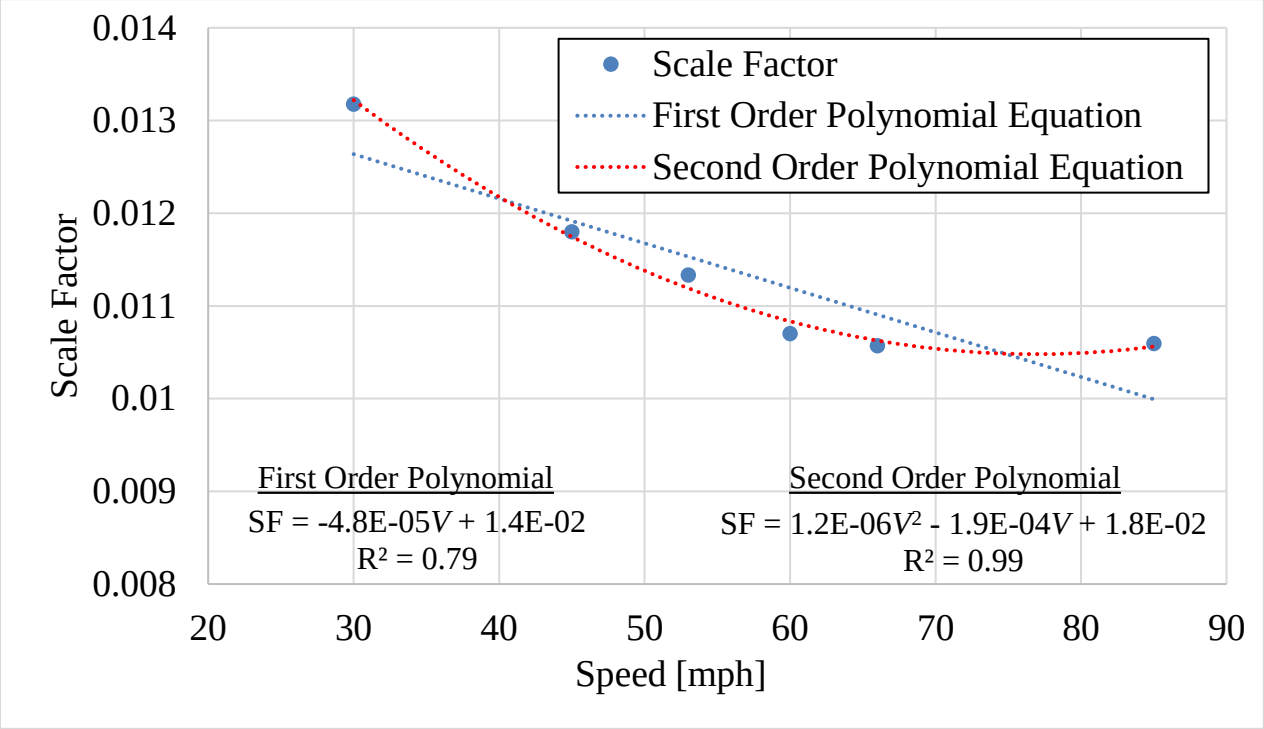

Figure 14: Laboratory data at 17% load used to correlate the cumulative bearing operating temperature difference above ambient to power consumption (4BT)

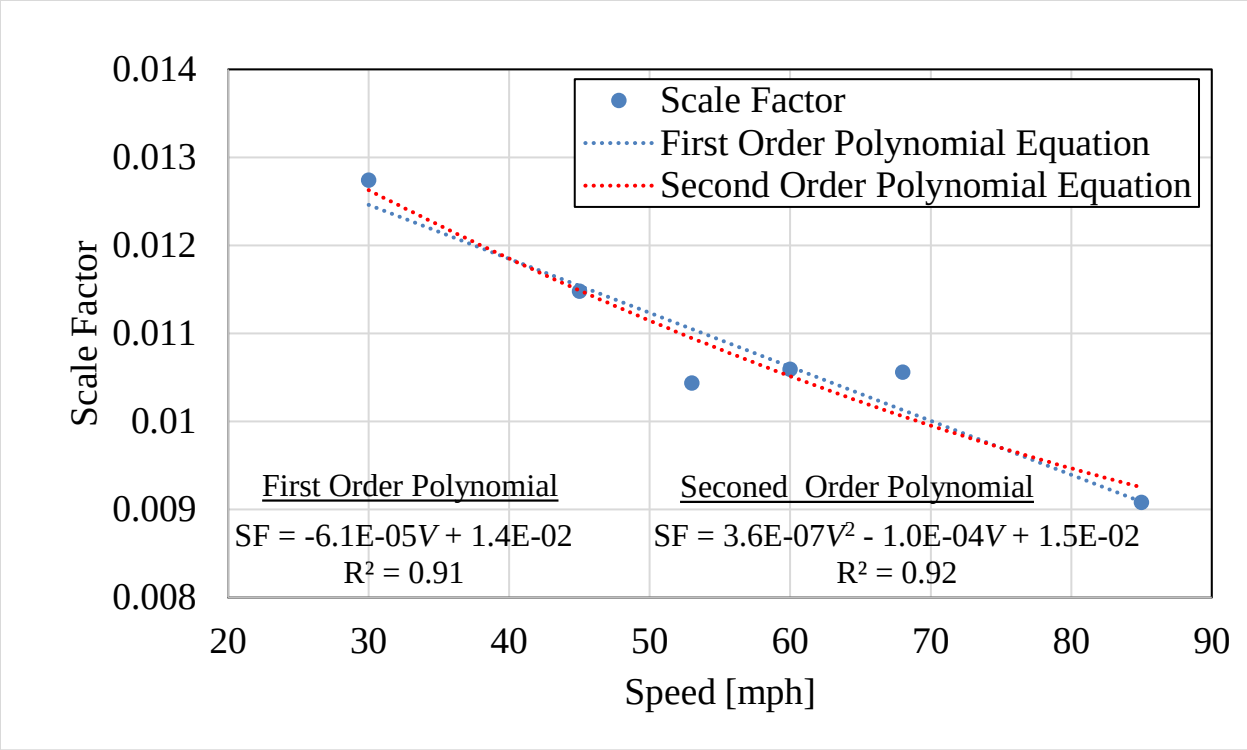

Figure 15: Laboratory data at 100% load used to correlate the cumulative bearing operating temperature difference above ambient to power consumption (4BT)

CHAPTER IV

RESULTS AND DISCUSSION

This chapter presents the correlations developed for the estimation of bearing power consumption along with a detailed analysis of the effectiveness and accuracy of these models. This study utilizes an array of class K and class F bearing data that was collected using two dynamic four-bearing testers, one of which is housed in an environmental chamber where the climate can be controlled.

4.1 Effect of Operating Conditions on Motor Power Consumption

4.1.1 Simulated Train Speed

In the laboratory, train speed is simulated through the axle rotational speed produced by the variable speed motor which is controlled through the variable frequency drive (VFD). To analyze the effect of the simulated train speed on motor power consumption, four class K control (defect-free) bearings were run on the dynamic four-bearing tester (4BT) under 17% load (26 kN or 5.85 kips per bearing) simulating an empty railcar traveling at simulated train speeds of 48, 72, and 97 km/h (30, 45, and 60 mph). The motor power profiles for these tests are plotted in Figure 16. As expected, the motor power consumption increased with an increase in the simulated train speed.

Further examination of Figure 16 reveals that the motor power, for all three speeds, approaches steady state conditions after the initial two hours of operation. For this reason, data pertinent to the initial two hours of operation was excluded from the analyses performed in this

study. Hence, the motor power values of this experiment, listed in Table 5, reflect the mean motor power without considering the first two hours of operation. Note that the motor power for the 48 km/h (30 mph) speed exhibits the sharpest decrease in power consumption during the start-up two-hour period, which is not surprising considering that this iteration was the first one conducted in this experiment and the grease was freshly packed. Because fresh grease is more viscous than grease that has been broken-in through operation, a higher motor power is required to overcome the initial frictional viscous forces of the freshly packed lubricant. This was not the case for the other two iterations in this experiment since the grease had already been broken-in by the time the speed was increased.

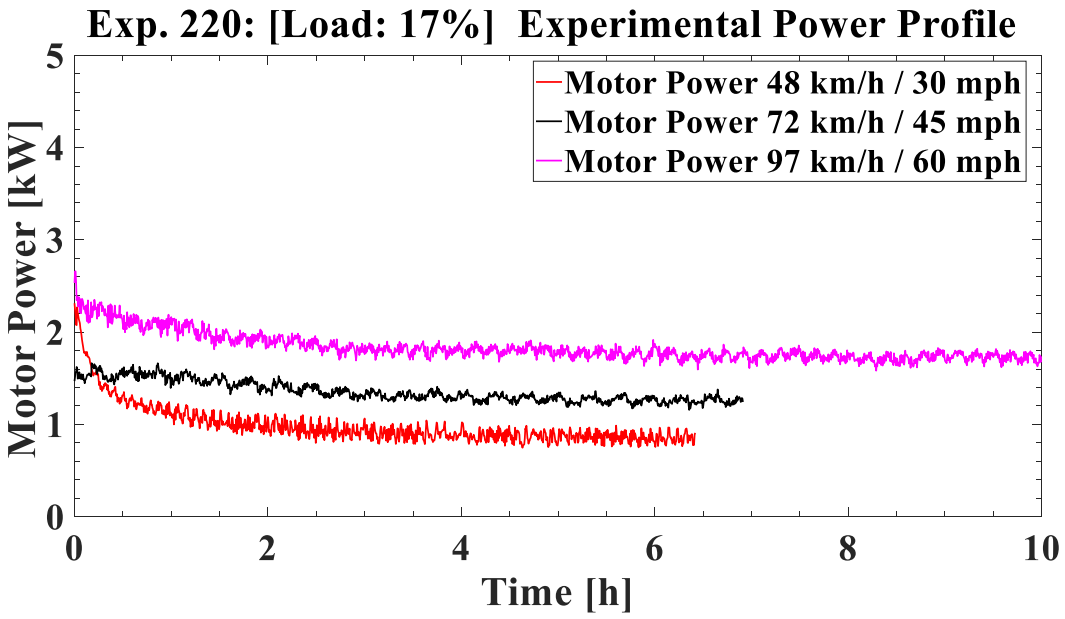

Figure 16: Motor power profiles at 17% load and speeds of 48, 72, and 97 km/h (30, 45, and 60 mph)

For better clarity of the data collected in Experiment 220, the motor power profiles given in Figure 16 were replotted in Figure 17 to display the steady state operation period only. The

mean motor power values summarized in Table 5 are representative of the motor power behavior presented in Figure 17.

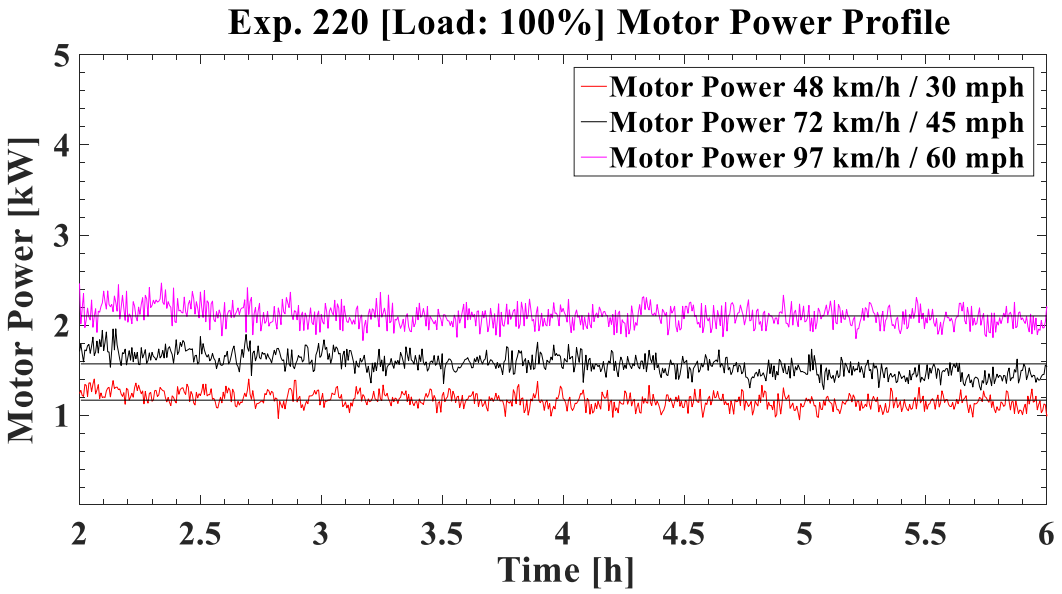

Figure 17: Motor power profiles at 17% load and speeds of 48, 72, and 97 km/h (30, 45, and 60 mph) showing period of interest

Table 5: Experiment 220 results at 17% load and speeds of 48, 72, and 97 km/h (30, 45, and 60 mph)

Exp. No.	Speed [km/h] / [mph]	Load	Bearing Class	Average Motor Power [kW]	Standard Deviation [kW]	MPG	$\frac{\text{ton} \cdot \text{mile}}{\text{gallon}}$
220	48 / 30	17%	K	0.81	0.09	525	1,536
	72 / 45			1.22	0.10	530	1,551
	97 / 60			1.64	0.11	524	1,533

Table 5 presents a summary of the results for the four-hour steady state duration of the experiment, which includes the following: average (mean) motor power, motor power standard deviation, miles per gallon (MPG), and ton-mile per gallon values. An evident trend that can be

observed by analyzing this table is that the average motor power increases with speed. Furthermore, by calculating the miles traveled at each speed over the four-hour period, the miles per gallon (MPG) and the ton-mile per gallon values were calculated for each of the three speeds using the relations presented in CHAPTER III of this thesis. The MPG and ton-mile per gallon values provide a theoretical measurement of efficiency for the miles traveled under a specific loading condition per gallon of diesel.

Interestingly, there was no significant difference in the MPG and ton-mile per gallon values for the three tested speeds at an empty railcar load. Yet, one can argue that the 72 km/h (45 mph) train speed is marginally more efficient for an empty railcar based on the slightly higher MPG and ton-mile per gallon values.

Table 6 lists the average operating temperatures above ambient for all four bearings on the test axle. The incremental change in the average operating temperatures above ambient between the three tested speeds was in the range of 10 to 12°C (18 to 22°F). An increase in the average operating temperatures of the test bearings accompanied the increase in speed. This behavior is expected as higher axle rotational speeds require additional motor power to overcome the added frictional forces, which manifests in elevated bearing operating temperatures.

Table 6: Average operating temperature above ambient results for Experiment 220 at 17% load (empty railcar) and speeds of 48, 72, and 97 km/h (30, 45, and 60 mph)

(Average ambient temperature was 20°C or 68°F)

Exp. No.	Speed [km/h] / [mph]	Load	Bearing Class	Average Operating Temperature Above Ambient			
				ΔT B1 [°C]	ΔT B2 [°C]	ΔT B3 [°C]	ΔT B4 [°C]
220	48 / 30	17%	K	22.0	20.4	21.4	19.5
	72 / 45			31.2	30.5	32.5	28.5
	97 / 60			43.4	43.0	42.7	41.4

Based on the observation that the average operating temperatures of all four test bearings were relatively similar at each of the three speeds, it was assumed that the average motor power consumption was equally distributed among all four test bearings. Under this assumption, the average power consumption per bearing was obtained by dividing the total power consumption given in Table 5 by four. Hence, the average power consumption per bearing at 17% load (empty railcar) was: 0.20 kW, 0.31 kW, and 0.41 kW for train speeds of 48, 72, and 97 km/h (30, 45, and 60 mph), respectively.

4.1.2 Simulated Railcar Load

Using the same experimental setup, the test rig was now set to 100% load (i.e., 153 kN or 34.4 kips per bearing) simulating a full railcar load, and the resulting motor power profiles for train speeds of 48, 72, and 97 km/h (30, 45, and 60 mph) were acquired. These profiles are plotted in Figure 18 with the average motor power consumption given in Table 7. Like the empty railcar tests, the average motor power consumption under full railcar load also exhibited an increase with operating speed. The results also revealed higher motor power consumption values for a fully

loaded railcar (100% load) compared to the corresponding values for an empty railcar (17% load) at each speed tested.

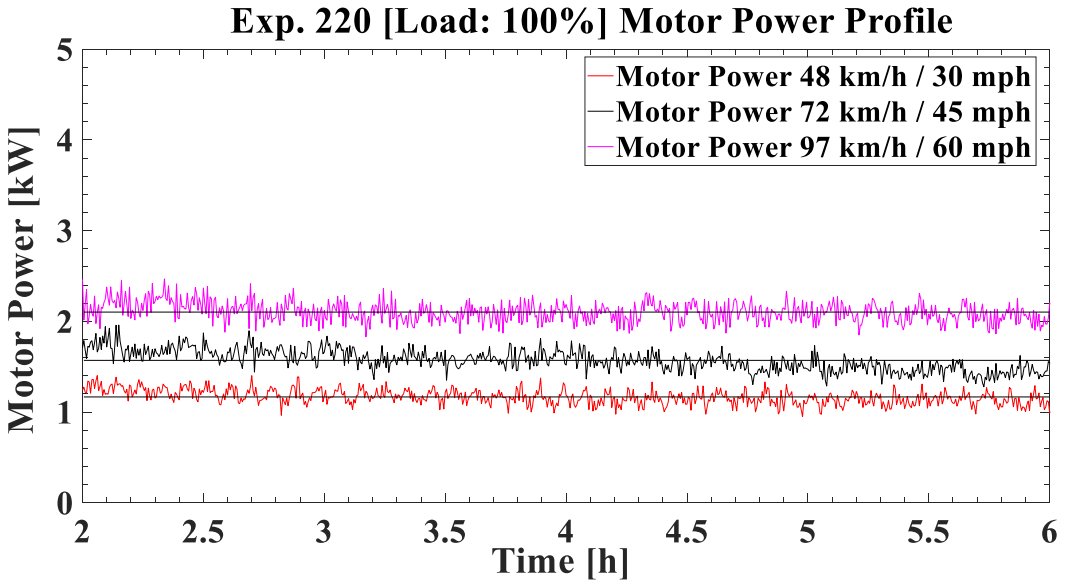

Figure 18: Motor power profiles at 100% load and speeds of 48, 72, and 97 km/h (30, 45, and 60 mph) showing period of interest

Table 7: Experiment 220 results at 100% load (full railcar) and speeds of 48, 72, and 97 km/h (30, 45, and 60 mph)

Exp. No.	Speed [km/h] / [mph]	Load	Bearing Class	Average Motor Power [kW]	Standard Deviation [kW]	MPG	$\frac{\text{ton} \cdot \text{mile}}{\text{gallon}}$
220	48 / 30	100%	K	1.17	0.10	366	6,302
	72 / 45			1.58	0.11	407	7,003
	97 / 60			2.10	0.13	410	7,047

Examining the results summarized in Table 7, one can notice that the ton-mile per gallon values for a fully loaded railcar are more than four times those for an empty railcar at all three

speeds investigated. Moreover, the MPG and ton-mile per gallon values for a fully loaded railcar indicate that there is a significant increase in efficiency going from a speed of 48 km/h (30 mph) to 72 km/h (45 mph), whereas the difference in efficiency going from 72 km/h (45 mph) to 97 km/h (60 mph) is negligible. Hence, speeds in the range of 72 km/h to 97 km/h are considered optimal in terms of fuel efficiency for a fully loaded railcar with healthy (defect-free) bearings.

More importantly, comparing Table 5 to Table 7, it becomes apparent that the ton-mile per gallon values provide a much better measure of fuel economy and efficiency than the MPG value. Even though the MPG values for a fully loaded railcar (100% load) are lower than the corresponding values for an empty railcar, the ton-mile per gallon values clearly demonstrate that a fully loaded railcar is more than four times as efficient as an empty railcar at all the three speeds investigated.

Table 8 provides the average operating temperatures above ambient for all four test bearings at a 100% load (full railcar) and speeds of 48, 72, and 97 km/h (30, 45, and 60 mph). As anticipated, the operating temperatures increased with train speed, and all the average operating temperatures for a fully loaded railcar were noticeably higher than those for an empty railcar at each of the three tested speeds. Moreover, the results indicate that there is a direct correlation between the motor power consumption and the operating temperatures of control (healthy) bearings.

Table 8: Average operating temperature above ambient results for Experiment 220 at 100% load (full railcar) and speeds of 48, 72, and 97 km/h (30, 45, and 60 mph)

(Average ambient temperature was 20°C or 68°F)

Exp. No.	Speed [km/h] / [mph]	Load	Bearing Class	Average Operating Temperature Above Ambient			
				ΔT B1 [°C]	ΔT B2 [°C]	ΔT B3 [°C]	ΔT B4 [°C]
220	48 / 30	100%	K	29.1	29.2	28.3	27.0
	72 / 45			35.3	36.8	37.8	35.2
	97 / 60			50.4	53.9	55.3	52.9

Once again, the average operating temperatures of all four test bearings were relatively similar at each of the three speeds. Hence, it was assumed that the average motor power consumption was equally distributed among all four test bearings. Therefore, the average power consumption per bearing at 100% load (full railcar) was: 0.29 kW, 0.40 kW, and 0.53 kW for speeds of 48, 72, and 97 km/h (30, 45, and 60 mph), respectively.

4.1.3 Bearing Condition

To explore the effects of defective bearings on fuel economy and efficiency, the outer ring (cup) of bearing B2 was replaced with a defective cup that had two relatively large spalls, pictured in Figure 19.

Figure 19: Bearing 2 (B2) cup spall
Spall 1 (left): Area = 1.575 in^2 ; Spall 2 (right): Area = 1.546 in^2

Like Experiment 220, Experiment 222 was run on the four-bearing test rig (4BT) under 100% load (full railcar) at simulated train speeds of 48, 72, and 97 km/h (30, 45, and 60 mph). The motor power profiles for all three speeds are plotted in Figure 20 and the results are summarized in Table 9.

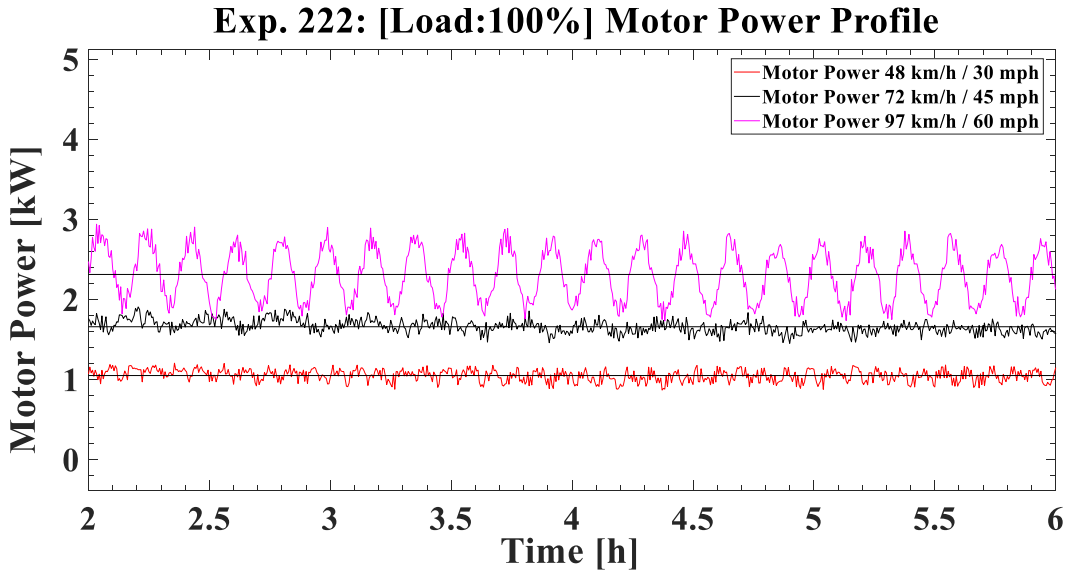

Figure 20: Motor power profiles at 100% load and speeds of 48, 72, and 97 km/h (30, 45, and 60 mph)

Table 9: Experiment 222 results at 100% load (full railcar) and speeds of 48, 72, and 97 km/h (30, 45, and 60 mph)

Exp. No.	Speed [km/h] / [mph]	Load	Average Motor Power [kW]	Standard Deviation [kW]	MPG	$\frac{\text{ton} \cdot \text{mile}}{\text{gallon}}$
222	48 / 30	100%	1.05	0.10	407	6,992
	72 / 45		1.67	0.11	386	6,631
	97 / 60		2.30	0.37	375	6,446

Examining Figure 20, a noticeable sinusoidal behavior is exhibited by the motor power at a speed of 97 km/h (60 mph). This behavior is also present at the lower speeds of 72 km/h and 48 km/h but to a significantly lesser degree. This sinusoidal behavior is caused by the defective bearing B2 which contains the two large spalls. The motor power profile suggests that the two spalls on the bearing cup are causing the tapered rollers to misalign resulting in an abnormal operating condition that generates more friction, thus, requiring a larger motor power consumption to overcome the additional frictional forces. The subsequent decrease in motor power consumption is the result of the rollers re-aligning and returning to normal operating conditions; hence, frictional forces are reduced.

By analyzing the average motor power, standard deviation, MPG, and ton-mile per gallon values listed in Table 9 and comparing them to the corresponding values for healthy (defect-free) bearings provided in Table 7, a marked increase in the average motor power consumption is observed for the defective bearing setup at the higher speeds of 72 km/h and 97 km/h. In contrast, the MPG and ton-mile per gallon values, which quantify the fuel economy and efficiency, respectively, decreased for the experiment running the defective bearing. Interestingly, the motor power standard deviation values seem to indicate that the effect of roller misalignment was more

pronounced at the highest speed of 97 km/h (60 mph). At the lower speed of 48 km/h (30 mph), the defective bearing did not adversely affect the fuel economy and efficiency. Quite the opposite, the MPG and ton-mile per gallon values were better for the defective bearing setup. This may be a result of the additional lubrication pockets that form in the spalled regions of the cup which assisted the motor in overcoming the frictional forces at the lower operating speeds. However, the negative effects of the spalls in the defective bearing manifest at the higher operating speeds where the frictional forces are greater.

The average operating temperatures above ambient for the four bearings in Experiment 222 are given in Table 10. Comparing the values of Table 10 to those for the healthy (defect-free) bearings listed in Table 8, at the two higher speeds (i.e., 72 and 97 km/h), the average operating temperatures of the bearings in the setup that contains one defective bearing (B2) are slightly higher than the corresponding bearing operating temperatures for the setup with no defective bearings (all four healthy bearings). At the lowest tested speed (i.e., 48 km/h or 30 mph), the average operating temperatures of the bearings in the setup with the one defective bearing are lower than those for the setup with all healthy bearings, for the reason explained earlier. This behavior agrees with the average motor power consumption values for both setups.

Table 10: Average operating temperature above ambient results for Experiment 222 at 100% load (full railcar) and speeds of 48, 72, and 97 km/h (30, 45, and 60 mph)

(Average ambient temperature was 20°C or 68°F)

Exp. No.	Speed [km/h] / [mph]	Load	Bearing Class	Average Operating Temperature Above Ambient			
				ΔT B1 [°C]	ΔT B2* [°C]	ΔT B3 [°C]	ΔT B4 [°C]
222	48 / 30	100%	K	26.7	27.5	28.8	25.5
	72 / 45			37.4	38.7	41.3	38.8
	97 / 60			52.3	53.3	58.5	53.1

* This was the defective bearing with the two spalls on its cup.

Even though the setup for Experiment 222 contained one defective bearing, the average operating temperatures of all four bearings in the setup were relatively close to one another at all three speeds. Hence, it can be assumed, within a reasonable approximation, that the motor power consumption is equally divided among all four bearings. Thus, the average power consumption per bearing at 100% load (full railcar) for a setup containing one defective bearing was 0.26 kW, 0.42 kW, and 0.58 kW for simulated train speeds of 48, 72, and 97 km/h (30, 45, and 60 mph), respectively.

4.1.4 Economic and Environmental Impact

The significance of bearing power consumption may be dismissed when looking at the relatively small experimental results from setups that only contain four bearings. Therefore, to quantify the fuel economy and efficiency resulting from the incremental changes in bearing power consumption, a simulation is proposed for a train consist of 59 wagons hauled by one locomotive. The results from this simulation are summarized in Table 11. To obtain the average power consumption values for the simulation presented in Table 11, the values listed in Table 7 and Table 9 were first multiplied by two to get the total power consumption per wagon, and then multiplied by 59 to obtain the total power consumption for the entire train consist. Similarly, the total tons hauled by this train consist were calculated by multiplying the full railcar (wagon) load of 143 tons (obtained from reference [1]) by 59 wagons. Note that using the values listed in Table 9 simulates a train consist having 25% defective bearings.

Table 11: Power consumption and energy efficiency of a simulated train consist of 59 wagons hauled by one locomotive

Simulation Results: 59 Wagons Hauled by One Locomotive					
Exp. No.	Speed [km/h] / [mph]	Load	Average Motor Power [kW]	MPG	$\frac{ton * mile}{gallons}$
220	48 / 30	100%	138	3.11	26,201
	72 / 45		187	3.45	29,112
	97 / 60		248	3.48	29,344
222	48 / 30	100%	124	3.44	29,065
	72 / 45		197	3.27	27,563
	97 / 60		272	3.18	26,794

Studying the results of Table 11, the optimal operating conditions for a 59-wagon train consist, assuming all bearings to be healthy, are fully loaded wagons with the locomotive traveling at speeds ranging from 72 km/h (45 mph) to 97 km/h (60 mph). However, traveling at a speed of 97 km/h (60 mph) with the train consist having 25% of its bearings defective will result in a 9% reduction in the fuel economy and efficiency as compared to a train consist with all healthy bearings traveling at the same speed.

4.1.5 Bearing Class

Using the chamber four-bearing tester (C4BT), Experiments 216B and 226C were performed to compare the performance of class F and class K control (healthy) bearings. For these experiments, the hydraulic cylinder of the test rig was set to apply 100% load (i.e., 153 kN or 34.4 kips per bearing) and the variable frequency drive (VFD) of the motor was set to a speed of 137 km/h (85 mph). The motor power profiles for these two experiments are plotted in Figure 21 with the results summarized in Table 12.

Examing Figure 21, it is evident that the setup with four class F bearings required noticeably higher motor power to rotate the test axle than the corresponding setup with four class K bearings. The disparity in motor power between the two bearing classes can be explained by the geometrical differences of the two bearing assemblies. As discussed in CHAPTER II , class F bearings have a wider outer ring (cup) than class K bearings because of the wider spacer ring region in class F bearings. Thus, the setup with four class F bearings require a longer test axle. Class F bearings weigh, on average, about 5.4 kg (12 lbs) more than class K bearings. Moreover, 266.2 mL (9 oz) of grease is applied to the spacer ring region of class F bearings while none is applied to the corresponding region in class K bearings. The added weight of the test axle with the four class F bearings coupled with the extra amount of lubricant applied to class F bearings are responsible for the higher motor power needed to run the setup at the same operating conditions as those for the class K bearing setup.

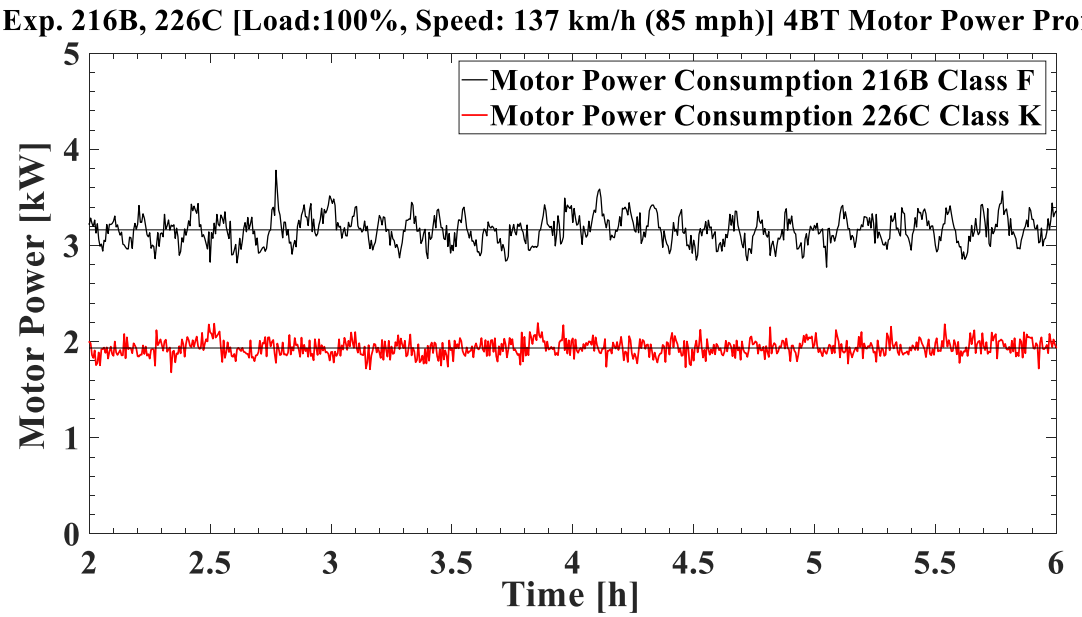

Figure 21 Motor power profiles at 100% load (full railcar) and 137 km/h (85 mph) for class F and K bearings

Looking at the values listed in class F bearings required 1.22 kW more power than class K bearings and had a 39% reduction in both MPG and ton-mile per gallon values. This significant difference in energy efficiency between the two classes of bearings further justifies the decision to have class K bearings replace class F bearings in rail service.

Table 12: Experiment 216B and 226C results at 100% load and a speed of 137 km/h (85 mph)

Exp. No.	Speed [km/h] / [mph]	Load	Bearing Class	Average Motor Power [kW]	Standard Deviation [kW]	MPG	$\frac{ton * mile}{gallons}$
216B	137 / 85	100%	F	3.16	0.19	135	2,328
226C			K	1.94	0.08	220	3,792

The results from Table 13 further verify the direct correlation between the average motor power consumption and bearing operating temperature. Because Experiment 216B (class F bearings) required a greater motor power, the corresponding bearing operating temperatures above ambient were also markedly higher than those in Experiment 226C (class K bearings). More importantly, this large discrepancy in bearing operating temperatures between the two classes of bearings can explain the increased number of false positives detected by HBDs in train consists that have railcars (wagons) with both classes of bearings.

Table 13: Average operating temperature above ambient results for Experiment 216B and 226C at 100% load and 137 km/h (85 mph)

(Average ambient temperature was 20°C or 68°F)

Exp. No.	Speed [km/h] / [mph]	Load	Bearing Class	Average Operating Temperature Above Ambient			
				ΔT B1 [°C]	ΔT B2 [°C]	ΔT B3 [°C]	ΔT B4 [°C]
216B	137 / 85	100%	F	48.5	57.9	47.5	52.5
226C			K	40.6	42.0	42.8	36.6

4.2 Bearing Power Consumption Estimation

The goal of this estimation is to provide the rail industry with a method to estimate the power consumption of freight train bearings in service. It is anticipated that this mathematical tool will aid railcar owners and railroads in making decisions regarding scheduling maintenance as it pertains to problematic bearings with high energy consumption.

4.2.1 Motor Power Estimation: Simulated Train Speed

Experiment 220, as previously described, was run at varying simulated train speeds of 48, 72, and 97 km/h (30, 45, and 60 mph) using class K control (i.e., healthy) bearings. The hydraulic cylinder was applied at 17% load (26 kN or 5.85 kips per bearing) and the four-bearing tester

(4BT) was used to perform this experiment. The resulting motor power profiles were plotted in Figure 22 with the developed motor power estimation correlation superimposed for comparison. Note that the developed motor power estimation correlation was explained in CHAPTER III.

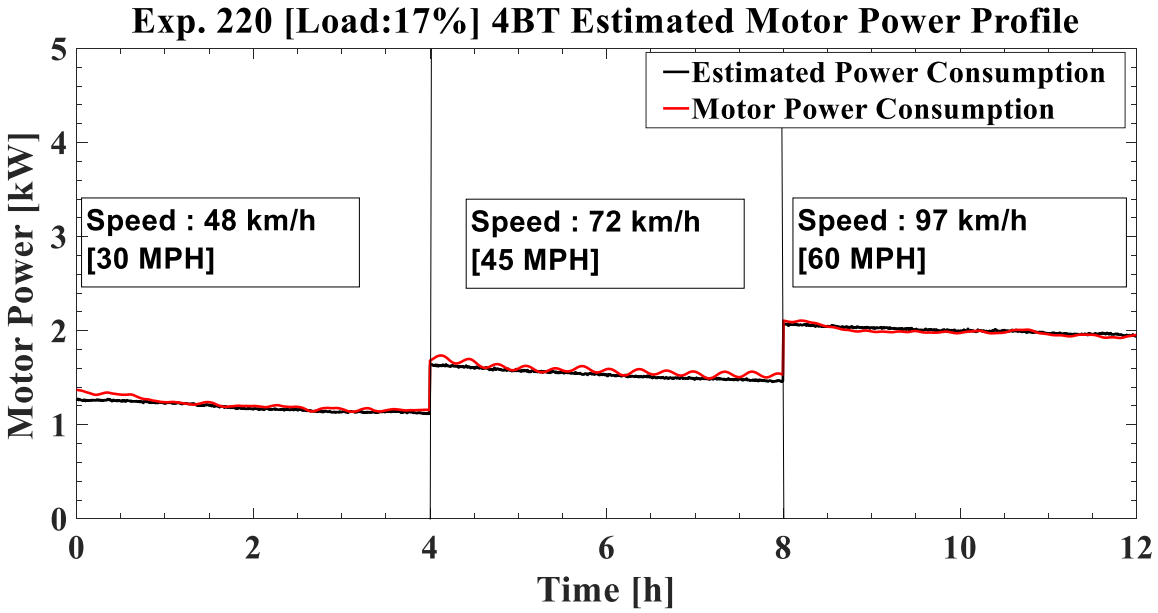

Figure 22: Motor power profiles at 17% load (empty railcar) and speeds of 48, 72, and 97 km/h (30, 45, and 60 mph) run on the 4BT using class K control bearings

Examining Figure 22, the following observations can be made regarding the accuracy of the estimated motor power correlation. First, as the motor power reaches steady state operating conditions for each tested speed, the alignment with the developed motor power estimation correlation improves. Moreover, it appears that the estimated motor power profile is steadier as it does not exhibit the small fluctuations present in the actual motor power profile. This behavior is more obvious in the motor power profile of the 72 km/h (45 mph) speed which exhibits a somewhat sinusoidal behavior while the estimated motor power displays a linear profile.

The results summarized in Table 14 demonstrate the accuracy of the devised motor power estimation correlation. The listed percent error calculations were obtained using Eq. (6) from

CHAPTER III. For each speed transition, the first two hours of data were excluded to allow for steady state operating conditions to prevail. All three speeds had the actual motor power and the estimated power matching exactly at several instances in the steady state regime, which explains the minimum percent error of 0%. Moreover, all three speeds displayed relatively low average percent errors, which validates the use of the scale factor technique utilized to develop the estimation correlation discussed in CHAPTER III. While the power estimation correlation had excellent goodness-of-fit R^2 values at speeds of 48 and 97 km/h (30 and 60 mph), the R^2 value for the 72 km/h (45 mph) speed was slightly lower. The lower R^2 value is attributed to the sinusoidal behavior of the actual motor power compared to the linear behavior exhibited by the estimated power profile.

Table 14: Experiment 220 results for motor power estimation at 17% load and speeds of 48, 72, and 97 km/h (30, 45, and 60 mph)

Exp. No.	Speed		Load	Percent Error [%]		Average Percent Error [%]	R^2
	km/h	mph		Minimum	Maximum		
220	48	30	17%	0.0	7.4	2.5	0.86
220	72	45		0.0	6.5	2.8	0.76
220	97	60		0.0	2.7	1.1	0.84

4.2.2 Motor Power Estimation: Simulated Railcar Load

Using the same experimental setup and following the same speed iterations delineated in Section 4.1.1 for an empty railcar load (17% load), the hydraulic cylinder of the test rig was set to apply 100% load (i.e., 153 kN or 34.4 kips per bearing) simulating a full railcar. The motor power profiles and summary of results for the simulated train speeds of 48, 72, and 97 km/h (30, 45, and 60 mph) are presented in Figure 23 and Table 15, respectively.

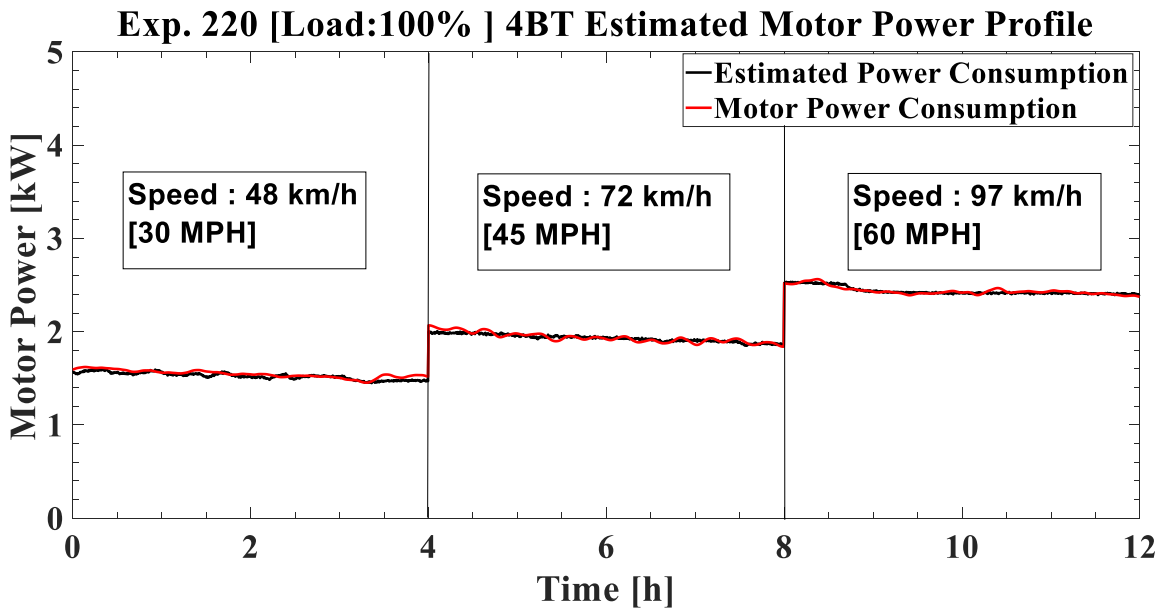

Figure 23: Motor Power Profile at 100% load (full railcar) and speeds of 48, 72, and 97 km/h (30, 45, and 60 mph) run on the 4BT using class K control bearings

Table 15 : Experiment 220 results for motor power estimation at 100% load and speeds of 48, 72, and 97 km/h (30, 45, and 60 mph)

Exp. No.	Speed		Load	Percent Error [%]		Average Percent Error [%]	R^2
	km/h	mph		Minimum	Maximum		
220	48	30	100%	0.0	4.8	1.7	0.62
220	72	45		0.0	4.1	1.1	0.87
220	97	60		0.0	2.5	0.6	0.77

Looking at Figure 22 and Figure 23, it is evident that the developed power estimation model effectively conforms to the different speed and load operating conditions. The agreement is particularly apparent at steady state operating conditions where the estimated power profile matches the actual motor power profile quite accurately. In fact, the accuracy of the developed

power consumption estimation model is demonstrated by the low average percent error (< 2%) for all speed and load operating conditions investigated. The goodness-of-fit R^2 values further support this conclusion.

4.2.3 Motor Power Estimation: Bearing Condition

Experiment 222 was performed on the four-bearing tester (4BT) using class K bearings under 100% load (full railcar load) and at simulated train speeds of 48, 72, and 97 km/h (30, 45, and 60 mph). However, for this experiment, the bearing occupying the B2 position on the test axle (refer to Figure 10 in CHAPTER II) had a defective cup with two relatively large spalls (see Figure 19). The motor power profiles for this experiment are provided in Figure 24 with the estimated power profiles juxtaposed. The summary of results can be found in Table 16.

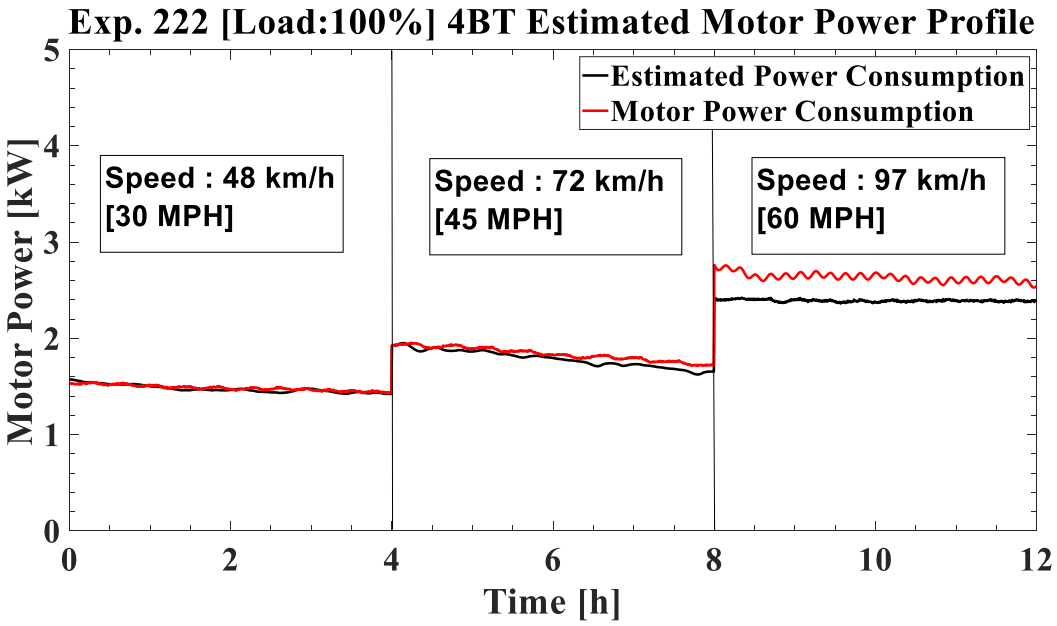

Figure 24. Motor power profiles at 100% load (full railcar) and speeds of 48, 72, and 97 km/h (30, 45, and 60 mph) run on the 4BT utilizing class K bearings (bearing B2 in this setup was

defective)

Table 16: Experiment 222 results for motor power estimation at 100% load (full railcar) and speeds of 48, 72, and 97 km/h (30, 45, and 60 mph)

Exp. No.	Speed		Load	Percent Error [%]		Average Percent Error [%]	R^2
	km/h	mph		Minimum	Maximum		
222	48	30	100%	0.0	4.1	1.1	0.81
	72	45		0.0	6.1	2.8	0.86
	97	60		6.1	13.6	9.6	0.16

Examining the profiles of Figure 24 Figure 16 and data of Table 16, the power estimation model accurately predicts the motor power at speeds of 48 and 72 km/h (30 and 45 mph), which is evident by the less than 3% average percent error and the excellent R^2 values. However, at the highest speed tested (97 km/h or 60 mph), the power estimation model underpredicts the actual motor power by as much as 0.36 kW (i.e., 13.6% error). Referring to Figure 20, one can recall that the effect of roller misalignment induced by the two large spalls on the cup raceway of bearing B2 did not manifest clearly until the speed was set to 97 km/h (60 mph). At that speed, the roller misalignment resulted in a noticeable sinusoidal motor power profile with the average motor power being higher than that required for healthy bearings and the fuel economy and efficiency being lower. Since the power estimation model was developed using scale factors calibrated with control (healthy) bearings, it underpredicted the actual motor power required to run a setup with one defective bearing. Nevertheless, the average percent error was less than 10%, which means that the model can still be used to predict the power consumption of defective bearings within a reasonable approximation.

4.2.4 Motor Power Estimation: Bearing Class

Since most freight railcars in North America utilize class F and K bearings, it is paramount to formulate a power estimation method that incorporates both bearing classes. Therefore, to accurately estimate the power consumption for each bearing class, separate scale factors were computed taking into account the difference in power consumption of the two bearings classes.

Experiment 216B was performed using four control (healthy) class F bearings under 100% load (153 kN or 34.4 kips per bearing) simulating a full railcar load at a train speed of 137 km/h (85 mph). To demonstrate what happens when the incorrect bearing class model is used to predict the power consumption, the actual motor power and estimated power consumption profiles of Experiment 216B were plotted in Figure 25 against the estimated power consumption obtained by applying the class K model (note that Experiment 216B used class F bearings).

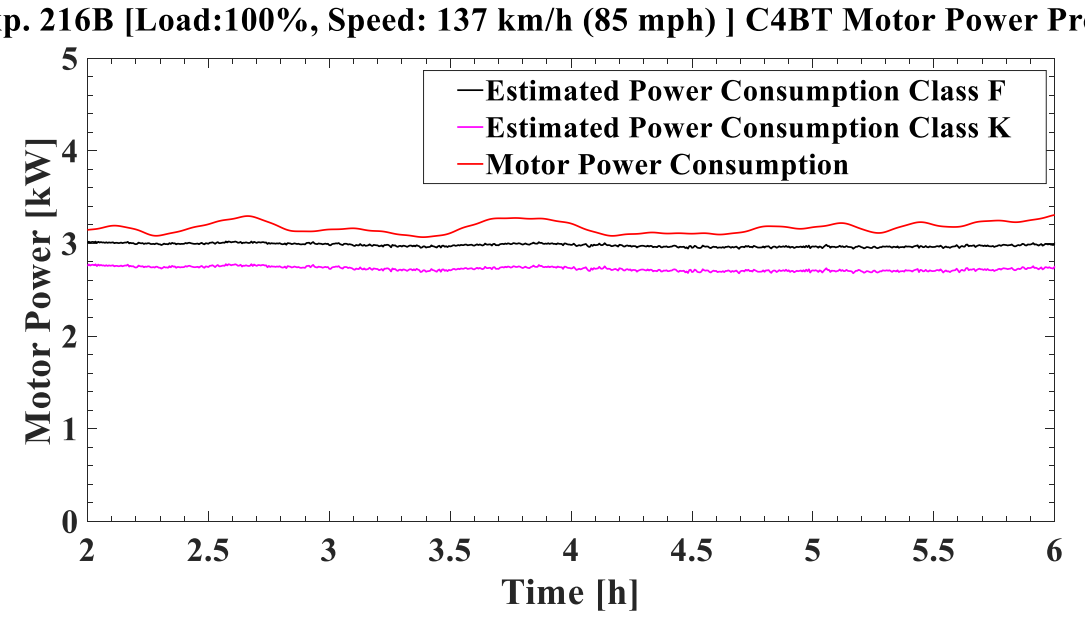

Figure 25. Motor power profiles at 100% load (full railcar) and 137 km/h (85 mph) run on the

C4BT using four class F bearings

Figure 25 contrasts the class F bearing power estimation profile, which is the correct bearing class used in this experiment, and the class K bearing power estimation profile. The percent error calculations are presented in Table 17. Examining the data, one can see that using the class K bearing model to predict the power consumption of class F bearings underpredicts the actual motor power by about 9% (average percent error), while using the correct class F bearing model yields estimates that are within 2% (average percent error) from the actual motor power. These results underscore the importance of using the appropriate bearing class model when predicting the power consumption. In rail service, knowing the number of class F and K bearings in a train consist is crucial in determining the most accurate estimates of total power consumption.

Table 17: Experiment 216B results for motor power estimation using different bearing class models (class K and class F) [100% load and a speed of 137 km/h (85 mph)]

Exp. No.	Bearing Class Model Used	Speed		Load	Percent Error [%]		Average Percent Error [%]	R^2
		km/h	mph		Minimum	Maximum		
216B	Class F	137	85	100%	0.0	12.8	2.2	0.47
216B	Class K	137	85	100%	1.9	31.3	8.6	0.47

CHAPTER V

CONCLUSIONS

There is an urgent need to identify, evaluate, and implement technologies and/or operating practices to maintain railroad competitiveness. This study focused on the energy consumption of a specific component – the railroad tapered roller bearing. The bearing power consumption was determined as a function of load, speed, bearing condition, and bearing class.

The results summarized throughout this thesis indicate that the ton-mile per gallon is a better measure of fuel economy and efficiency than the corresponding miles per gallon (MPG). This became apparent when comparing the values for an empty railcar (i.e., Table 5 versus a fully loaded railcar (i.e., Table 7 and Table 9). The reason for this is that the ton-mile per gallon metric incorporates both the MPG and the total cargo load haul. Interestingly, the motor power consumption did not directly correlate to the fuel efficiency of the train.

The results of the study also concluded that defective bearings can significantly affect the fuel economy and efficiency of the train, especially at the higher speeds (≥ 72 km/h or 45 mph). This finding is supported by the results of the simulation done on a train consist of 59 wagons (railcars) hauled by one locomotive where 25% of the bearings were defective. The results listed in Table 11 compared the fuel economy and efficiency of a train consist with all healthy bearings to that of the same train consist with 25% of its bearings being defective. This comparison revealed that the defective bearings were responsible for a 9% reduction in fuel efficiency at a

train speed of 97 km/h (60 mph). To quantify this reduction under a tangible field scenario, consider a 5,600-mile trip (round trip from New York, NY to Los Angeles, CA) hauling 59 fully loaded wagons at 97 km/h (60 mph). A train consist having 25% faulty bearings would require 153 gallons of diesel more than an equivalent train consist with all healthy bearings.

Additionally, the results conclude that class F bearings require, on average, 39% more power to run at the same load and speed conditions as class K bearings, as demonstrated in Table 12. The additional 5.4 kg (12 lb) weight of the class F bearing coupled with the extra 266.2 ml (9 oz) of lubricant packed in the spacer ring region of the bearing contribute to the increased power required to run class F bearing. Hence, the decision to have class K bearings replace class F bearings in rail service can be justified by the improved fuel economy and efficiency.

Furthermore, the results summarized for the motor power estimation tool demonstrated that models can be devised to provide accurate estimates of the power consumption of railroad bearings with an average percent error of less than 10% for the different parameters investigated which include: speed, load, bearing class, and bearing condition. Nevertheless, the models can be further improved and optimized through additional experimentation, especially tests performed to explore different bearing conditions other than the spalled cup scenario investigated in this study.

The proposed power consumption estimation models developed in this study present a first step towards constructing a feasible power estimation methodology that can be applied in the railway industry to determine bearing power consumption in real-time. These models can also inform railcar owners and railroads about bearings that might be consuming more energy so a closer inspection or a timely maintenance service can be scheduled.

This thesis summarizes the preliminary work conducted to demonstrate how the performance of railroad tapered-roller bearings can affect the fuel economy and efficiency of a train under normal and abnormal operating conditions. The acquired results provide the reader with a basic understanding of how incremental changes in bearing power consumption affect the overall fuel economy and efficiency. A new methodology for estimating the power consumption of railroad bearings is introduced, which can aid the railway industry in maintaining a competitive edge by optimizing the fuel economy and efficiency of their trains. Note that the effects of drag were not considered in the presented analyses and further work is needed to evaluate the effects of drag forces on fuel economy.

REFERENCES

[1] Tolliver, D., Lu, P., and Benson, D., (2013). Analysis of Railroad Energy Efficiency in the United States. MPC Report No. 13-250. [online] Available at: https://www.ugpti.org/resources/reports/downloads/mpc13-250.pdf [Accessed 5 November 2019]

[2] Csx.com. (2019). CSX.com - Fuel Efficiency. [online] Available at: https://www.csx.com/index.cfm/about-us/the-csx-advantage/fuel-efficiency/?mobileFormat=true

[3] How Technology Drives the Future of Rail. (2020, August 25). Retrieved January 04, 2021, from https://www.aar.org/article/the-future-of-rail/

[4] Gao, Z., Lin, Z. and Franzese, O. (2019). The energy consumption and cost savings of truck electrification for heavy-duty vehicle applications. [online] Osti.gov. [Accessed 7 March 2017].

[5] Orfe.princeton.edu. (2015). Automated Driving and Platooning Issues and Opportunities. [online] Available at: https://orfe.princeton.edu/~alaink/SmartDrivingCars/ITFVHA15/ITFVHA15_USA_FutureTruck_ADP_TF_WhitePaper_Draft_Final_TF_Approved_Sept_2015.pdf [Accessed 21 September 2015].

[6] Zhang, L., Chen, F., Ma, X., & Pan, X. (2020, January 03). Fuel Economy in Truck Platooning: A Literature Overview and Directions for Future Research. Retrieved November 08, 2020, from https://www.hindawi.com/journals/jat/2020/2604012/

[7] Fatality Facts 2018: Large trucks. (n.d.). Retrieved November 08, 2020, from https://www.iihs.org/topics/fatality-statistics/detail/large-trucks

[8] Train Fatalities, Injuries, and Accidents by Type of Accident. (n.d.). Retrieved January 04, 2021, from https://www.bts.gov/content/train-fatalities-injuries-and-accidents-type-accidenta

[9] Duan, D. (2017, November 23). Truck Platooning: The Band of Semi-Trailers: Chemistry And Physics. Retrieved November 09, 2020, from https://www.labroots.com/trending/chemistry-and-physics/7405/band-semi-trailers-truck-platooning

[10] ICF International (2019). Comparative Evaluation of Rail and Truck Fuel Efficiency

on Competitive Corridors. Available at: www.fra.dot.gov/Elib/Document/2925

[11] Liu, Xiang, M. RapikSaat, and Christopher PL Barkan. "Analysis of causes of major train derailment and their effect on accident rates." Transportation Research Record 2289.1 (2012): 154-163.

[12] https://www.schaeffler.my/remotemedien/media/_shared_media/08_media_library/01_publications/schaeffler_2/brochure/downloads_1/pbs_de_en.pdf

[13] Lindgreen, E. B. G., & Sorenson, S. C. (2005). Simulation of Energy Consumption and Emissions from Rail Traffic. Technical University of Denmark. Department of Mechanical Engineering. MEK-ET-2005-04

[14] "Thermal Analysis of Railroad Tapered Roller Bearings," by Fadi Alnaimat, December 2007.

BIOGRAPHICAL SKETCH

Carlos Eliasar Lopez III was born in McAllen, Texas, US, on November 2, 1994. Carlos Lopez was a graduate student at the University of Texas Rio Grande Valley (UTRGV) where he obtained his bachelor's degree in Mechanical Engineering. He has worked for the University Transportation Center for Railway Safety (UTCRS), directed by Dr. Constantine M. Tarawneh, for four months. Mr. Lopez one of the leaders for the manufacturing of the SAE Baja Racing car and he is the leader for railroad bearing power consumption project. In addition, he has significant design experience in HVAC systems and worked experience with HM3 Engineering Consultants for four years. In addition, he had a summer internship with Cummins in Fridley, Minnesota. He earned a Master of Science in Mechanical Engineering from the University of Texas Rio Grande Valley in December 2020. Carlos E. Lopez III can be reached at c3lopez65@gmail.com.